MARCHE POLYTECHNIC UNIVERSITY

ENGINEERING FACULTY

Master's degree in biomedical engineering

NUMERICAL SIMULATION OF BLOOD FLOW IN THE CAROTID BIFURCATION WITH PLAQUES

Degree thesis by:

Valentino D'Egidio

Supervisor:

Maurizio Brocchini

Co-Supervisor:

Gianluca Zitti

Accademic year 2021/2022

Summary

ABSTRACT

The evaluation of the properties of large arteries, such as wall remodeling, distensibility and stiffness in individuals with cardiovascular (CV) risk factors, can represent a valid approach to monitoring preclinical alterations that precede the development of atherosclerotic lesions. From numerous studies conducted, it has emerged how altered values of the Wall Shear Stress (WSS) are responsible for the expression, by endothelial cells, of a genetic profile proatherogenic potentially able to favor the development of atherosclerotic lesions. In particular, a non-laminar oscillatory flow pattern, as has been observed in the vicinity of the bifurcations and curvatures of the vessels, causes an alteration of the shear stress, a condition capable of exerting a pro-atherogenic effect.

This thesis aims to reproduce the blood flow inside the carotid artery, in particular in the area of the bifurcation, making use of numerical simulations performed by means of the Ansys Fluent 19.2 software. The flow was simulated in the presence of atherosclerotic plaques of different sizes in the area of the carotid bulb, the area at greatest risk of developing these plaques. We then focused on the study of the WSS in different areas of interest present on the artery wall and how it varies according to the extent of the occlusion, using plaques of 3,2 and 1mm thickness. A parameter has been estimated, i.e. the resistance, which intrinsically provides information on the flow and pressure. The case with the 3-mm plates presents results different from those of the 2-mm and 1-mm plates, which are much more similar to each other. In particular, it was observed that the case with 3-mm plates, in addition to being the only one that presents maximum WSS values on the plaque rather than in the bifurcation area, has higher mean WSS values in the bifurcation area if compared to a healthy case, 8% as peak of maximum variation, while the two reduced obstructions present a maximum negative variation of 6%, although the 1-mm plaques case appears to have a greater average variation than the 2-mm ones. The same variation trend is maintained only in the internal carotid artery where, however, the case with 3-mm plates presents much greater variations (-19%) than those with 2-mm plates, which show a maximum negative variation of the 7%, while the smallest shows a more or less constant variation of 4%. At the wall of the external carotid we instead observe an increase in the mean WSS values of up to 20% in the case of 3-mm plaques, while we find a more or less comparable decrease in the mean WSS in the other two occlusions, with a maximum negative variation of 9 %. The 3-mm occlusion is also unique in having significant velocity redistribution, increasing velocity in the artery where the occlusion is not present. According to the estimated resistive parameters, the resistance R1 should rise as occlusion rises. In contrast, the R2 resistance does not appear to follow a linear trend; rather, the case with 3-mm plaque exhibits an increase in comparison to the healthy case, while that of the two minor obstructions exhibit a decrease, which is more pronounced in the case of 1-mm thick plaques. R3, however, decreases both for 3-mm plates and for 2-mm and 1-mm plates, with the latter having values that are comparable to one another and more like the healthy case.

The minor variations of the smaller plates with respect to that of the larger plates, may be attributable to the fact that, in the case of smaller plaques, there is no significant redistribution of the velocity in the system, maintaining a behavior more similar to the healthy case, and in particular the speed near the walls does not change significantly, although in any case the average speeds show some variations.

These simulations moreover demonstrate how the non-consideration of the elastic wall does not allow us to carry out a real study of the parameters in consideration, however they give us information on how much the mere modification of the geometry has significant effects on the parameters in consideration.

CHAPTER 1- INTRODUCTION

Introduction

The purpose of this thesis is primarily to simulate the flow inside the carotid bifurcation considering an input velocity as a function of the cardiac cycle, blood properties and pressure values as boundary conditions. After that, two plates were then inserted in the area of the carotid sinus, the dimensions of which were then varied so as to be able to study the trend of the quantities of interest such as speed, resistance and WSS which is evalueted in the bifurcation area and on the internal and external carotid artery walls, according to the dimention of the plaques.

1.1 Cardiac Cycle

In order to study the fluid dynamics in the carotid artery, it is first necessary to introduce the cardiac cycle, as the source of the flow itself. Figure 1 shows the cardiac cycle, which is composed of a relaxation period that it is called diastole, during which the heart fills with blood, followed by a period of contraction called systole, in which the heart empties. [1] The figure shows that the beginning of the cardiac cycle is given by atrial and ventricular diastole, this implies that both the atria and the ventricles are relaxed and there is the filling of the ventricles. Later, atrial systole occurs which pushes an additional amount of blood into the ventricles, then there it is the ventricular systole which is divided into two phases; in the first phase there is the closure of the atrioventricular valves, the first heart sound is produced and in the second phase the ventricular pressure increases, the semilunar valves open and there is the push of the blood in the arteries. Finally, there is the ventricular diastole where the ventricles relax, the semilunar valves close and the second heart sound is produced. [1]

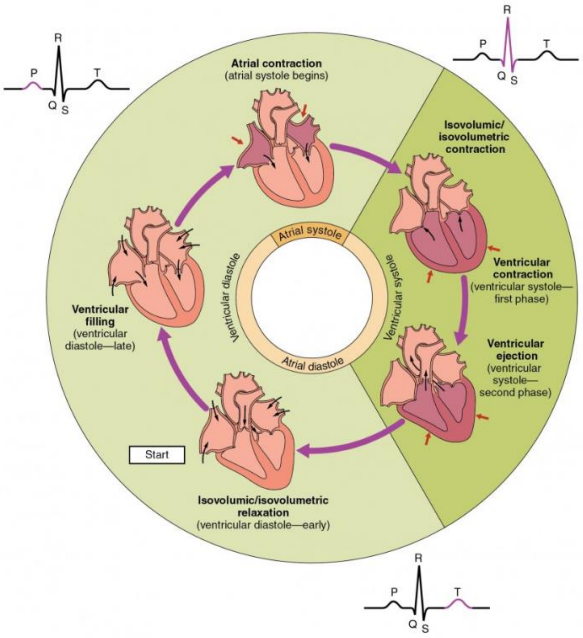

Figure 1. The cardiac cycle[1].

Therefore, the cardiac cycle can be defined as the succession of two periods, systole and diastole. In turn, they are divided into phases, which are: isovolumetric contraction, ejection, isovolumetric relaxation, rapid filling, diastasis, and atrial systole. This is well represented in the Wiggers diagram, in Figure 2, where the different events during the cardiac cycle are shown in the left side of the heart.

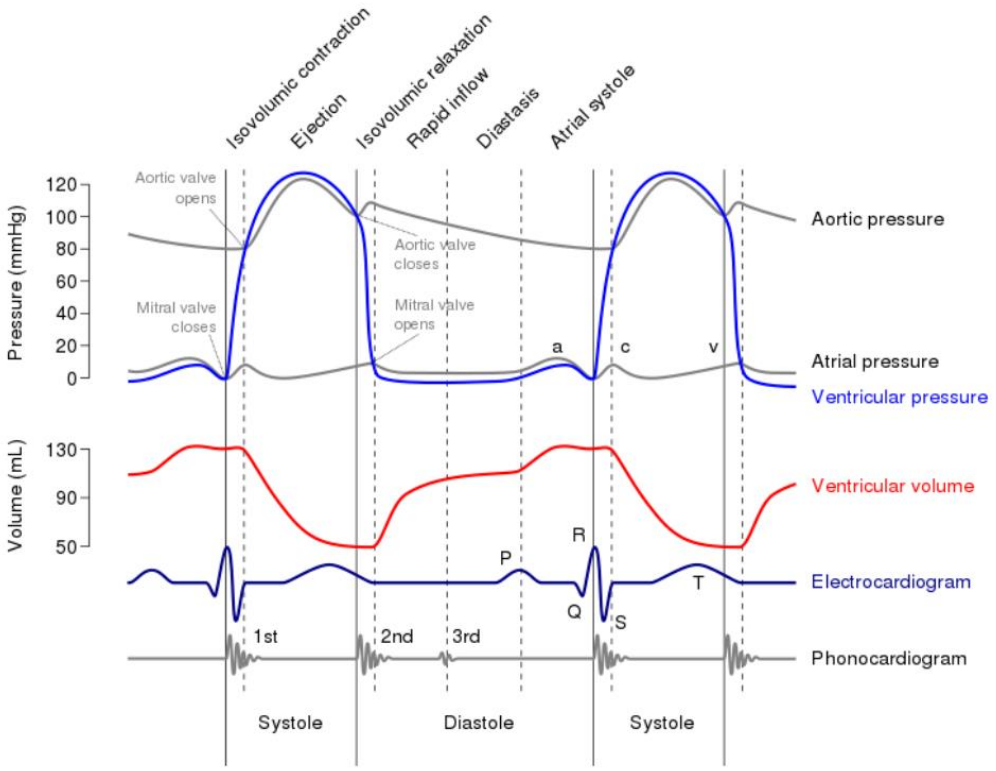

Figure 2. Wigger's diagram of the left side of the heart[2].

The first three curves depict the varying pressures in the left atrium, aorta, and left ventricle. The left ventricle volume changes are defined by the fourth curve, the ECG by the fifth, and the phonocardiogram by the sixth, which reproduces the sound made by the heart pump, primarily by the heart valves[2].

The many cardiac cycle stages for the left ventricle's operation may also be shown in Figure 2. The mitral valve closes as a result of an increase in intraventricular pressure during isovolumetric contraction. Furthermore, the ventricular chamber is currently closed as the mitral valve and those of the aorta is also closed. The pressure is 80 mmHg at the conclusion of this phase, a pressure value that the ventricle must overcome in order for the aortic valve to open and allow for blood ejection in the aorta. When the aortic valve opens, which occurs during the ejection phase, there is a reduction in ventricular capacity and a rise in the aortic pressure; The peak pressure ranges from 125 to 130 mmHg. When the ventricular volume curve reveals a slowing of the outflow rate, the subsequent ejection phase starts and concludes with a pressure of around 100 mmHg.

In the second phase, there is a decrease in intraventricular pressure that culminates with the closure of the aortic valve, and the conclusion of the systole, at this time the first portion of the second of the heart sounds is heard.

The aortic semilunar valves close, the second tone occurs, and blood pressure decreases until it reaches zero during isovolumetric relaxation to allow blood to flow from the atrium, a low-pressure chamber, to the ventricle, a high-pressure chamber.

The ascent of the ventricular volume curve and the opening of the mitral valve occur simultaneously during the ventricular fast-filling phase. The sluggish filling phase, or diastasis, is recognized by a little deviation in the ventricular volume curve that is linked to the third tone, a low-frequency vibration. The atrium and ventricle's pressures gradually rise, causing the ventricle to passively fill up until the atrial systole which may be heard as the fourth heart sound and the 'a' wave of the atrial pressure trace intervenes [3].

1.2 Arteries

The arteries and the blood are the other two primary parts of the circulatory system. Arteries are strong, elastic tubes that carry blood while being subjected to the heart's intense pumping pressure. In the human body, arteries primarily control the flow of oxygen, nutrients, and hormones. After loading fresh oxygen in the core of hemoglobin, arteries carry oxygenated blood throughout the body. The oxygen is then released through capillaries, which are high-surface areas with a change in affinity for the oxygen. Figure 3 illustrates how the branches of the aorta, which is the largest artery in the human body, gradually get smaller before reaching the level of the capillaries.

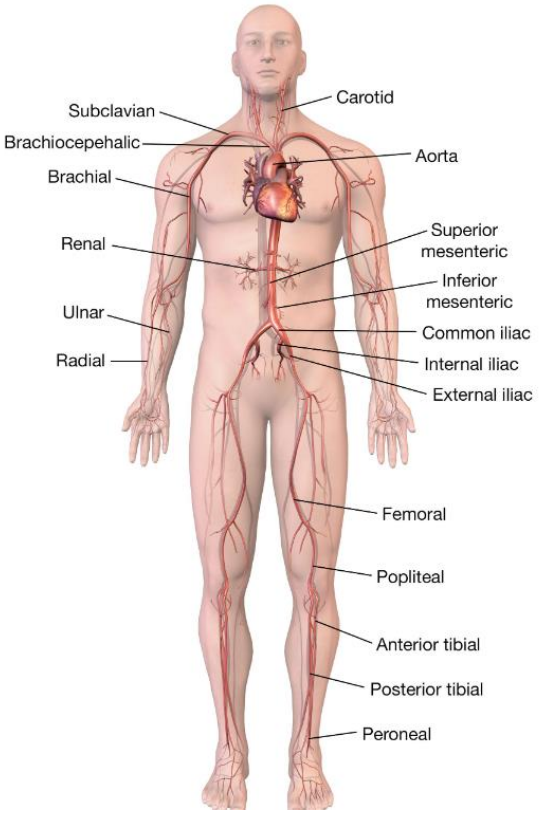

Figure 3. Main ramifications of the aorta, which emerges from the heart's left ventricle and carries oxygenated blood to all parts of the body reached by the systemic circulation [4].

The values and fluctuations of blood pressure vary greatly depending on the distance they have from the heart.In Figure 4 is shown the time-averaged pressure over a cardiac cycle measured in different sections of the systemic circulatory system. It can be seen in fact, that pressure amplitude and fluctuation decrease moving away from the heart coinciding with a decrease in the diameter of the vessels [5].

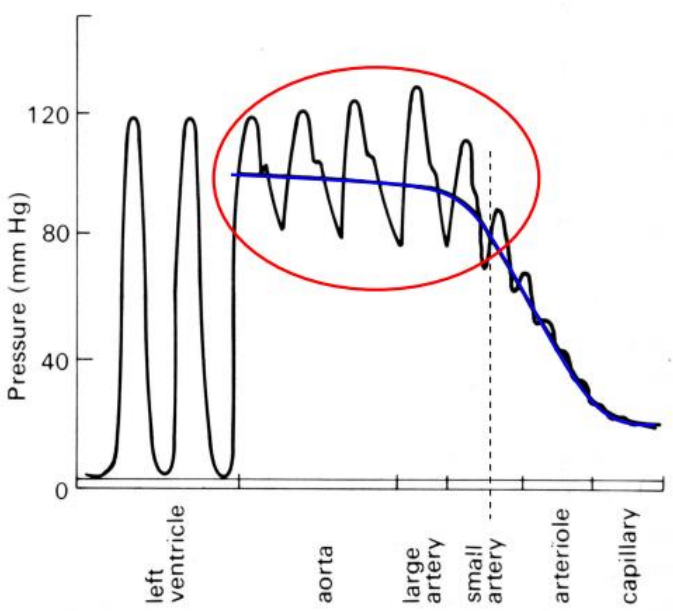

Figure 4. Dynamic pressure and its mean level (blue line) in the arterial circulation [5].

The growth of the amplitude of fluctuations along the aorta (within the red circle) is due to a wave reflection phenomenon [5]. Like the pressure, the flow also fluctuates in large arteries, therefore the flow is also unsteady. In particular, as shown in figure 5, where a simultaneous recording of both aortic pressure and flow is reported, the pressure and flow waveforms are seen to be fairly similar in the systolic phase but clearly different during diastole [6].

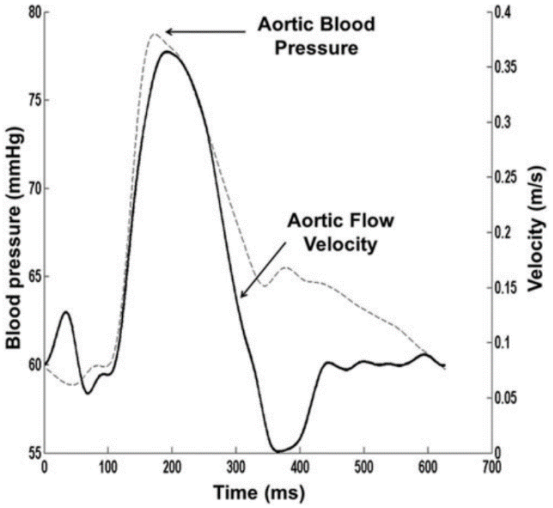

Figure 5. Example of averaged (6 beats) aortic blood pressure (broken line) and aortic flow velocity (solid line) recorded during coronary artery bypass graft surgery [6].

1.2.1 Artery's wall

Although there are variations in the composition of the walls, the arterial wall always consists of three concentric tunics:

-Tunica intima: This is the first most inner layer of the artery, is made up of a smooth muscle layer that contains one layer of endothelial cells, in direct contact with the blood. The tunica intima acts as a conduit, allowing oxygen-rich blood to go to the proper perfusion location. This prevents leakage from the artery, allowing the nutrient-rich blood to get to the desired location before releasing its oxygen and other nutrients.

-Tunica media: Tunica media is made up of smooth muscle cells, elastic tissue and collagen. It lies between the tunica intima on the inside and the tunica externa on the outside. Its structure varies according to the size of the artery, In the largest arteries, such as the aorta, there is a significant amount of elastic tissue. The muscular fiber cells have well-marked, rod-shaped nuclei that are frequently slightly bent and are grouped in 5 to 7 layers of circular and longitudinal smooth muscle with a length of around 50µm.

-Tunica externa: Is the outermost tunica of a blood vessel. Collagen makes up the majority of it, and in arteries,works as an external elastic support. Collagen, in fact, gives the blood artery stability by serving as an anchor to adjacent organs.

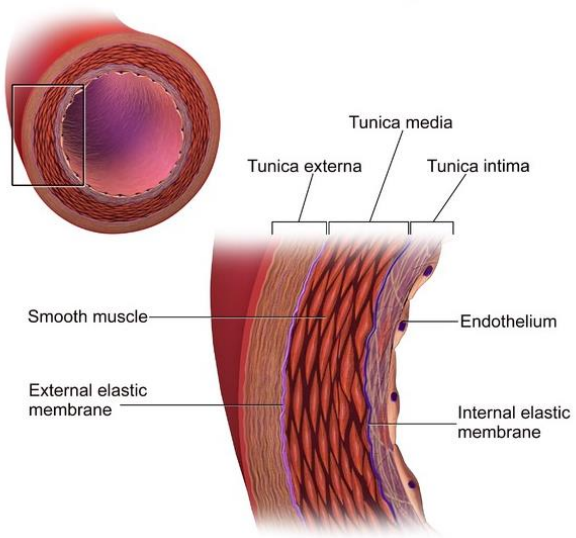

Figure 6. Section of an artery in which the different layers of the arterial wall are shown [7].

The elastic properties of the vessels, therefore, vary greatly according to the composition of the walls, and therefore according to their diameter. Elastic tissue predominates in the medium tunic of large caliber arteries (diameter from 3 cm to 7 mm), whereas muscle tissue predominates in the medium and small tunic (diameter from 7 mm to 0.2 mm) arteries. Therefore, we make a distinction between arteries of the elastic and muscular types: whereas the latter (medium and small caliber arteries) have a contractile wall and are therefore able to actively vary their lumen, thereby regulating the amount of blood that flies through them, the elastic ones instead (large-caliber arteries) have an elastic wall and passively intervene in the blood circulation: they dilate during ventricular systole and, in the diastolic phase of the cardiac cycle, return, due to the elastic energy accumulated, to the original size. In particular, it has been shown that for larger vessels, the variation in diameter occurs in phase with pressure, thus making them not dissimilar to an elastic material [8]. The Winkessel effect, which occurs in correspondence with the largest arteries, is due to the strong elastic component of the walls. This physiological phenomenon allows to modify the discontinuous flow of the cardiac output into a more continuous flow, transforming the kinetic energy of the blood coming from the left ventricle into elastic potential energy. During systole we witness the elastic dilation of the walls of the aorta and of the large vessels thanks to vascular compliance. A part of the systolic range is thus “storage”. This amount of blood will then be used, in the diastole phase, to ensure continuity of flow even in the absence of ventricular pumping.

1.2.2 Carotid artery

One of our body’s largest and most significant arterial trunks, the carotid artery is primarily in charge of vascularizing the head and neck. The common carotid artery is the primary branch of the carotid artery, which later separates into the internal and external carotid arteries. On the right side of the body, the common carotid artery originates from the brachiocephalic artery, whereas on the left, it comes directly from the aorta. The internal and external carotid arteries split off from the common carotid artery at the height of the larynx. The superficial temporal artery and internal maxillary artery are the external carotid artery’s terminal branches. The external carotid artery starts between the third and fourth cervical vertebrae. On the other hand, the internal carotid artery ascends to the petrous rock of the temporal bone, where it enters the cranial cavity, passes the cavernous sinus, and finally terminates beneath the anterior perforated substance. The

anterior cerebral artery and middle cerebral artery are its terminal sections. In figure 7 a sagittal section can be seen in which the course of the right carotid artery is shown.

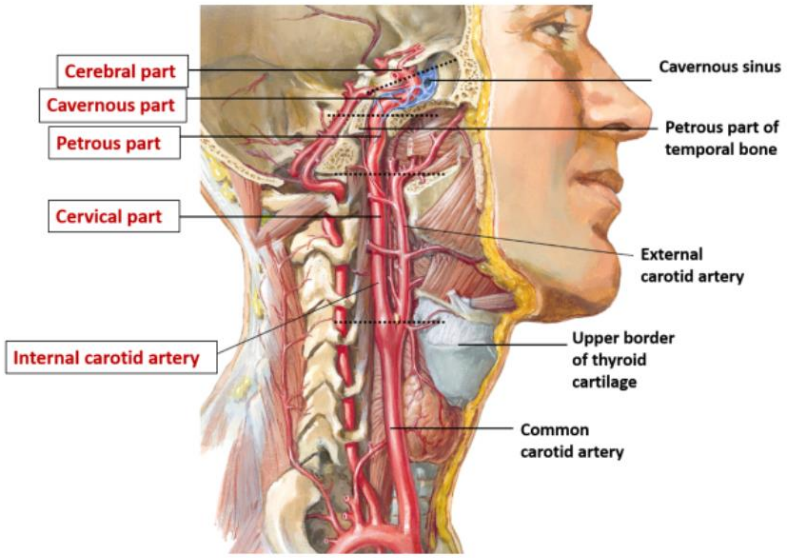

Figure 7. Sagittal section showing the course of the right carotid artery. It can be seen how this originates from the brachiocephalic artery before dividing into the internal and external carotid artery [9].

Common carotid artery lumen diameter ranges from 4.3 mm to 7.7 mm. No differences are noted between the left and right common carotid artery lumen diameter (5.78 +/- 0.57 mm and 5.86 +/- 0.66 mm), and the internal and external carotid artery lumen diameter as well. Although common carotid artery intima-media thickness is similar in comparison between left and right and both sexes, several studies have shown that the lumen of the carotid arteries is smaller in women [10]. An area of particular importance is the carotid bulb. The carotid bulb, or carotid sinus, is a neurovascular structure that develops as a dilatation at the point where the internal carotid artery and common carotid artery split in two. It is situated at the level of the thyroid cartilage, inferior to the angle of the jaw, close to the arterial pulse. Baroreceptors (stretch receptors), which are sensitive to variations in arterial blood pressure, are found in this area. Also from a fluid dynamic point of view, this area is very important, in this area the flow, in fact, passes from the laminar state to the turbulent one. In laminar flow, unlike turbulent flow, the infinitesimal layers of fluid flow smoothly one above the other, without any mixing, not even at a microscopic level. Precisely because of this separation of flows, the carotid sinus is one of the most common sites for the onset of atherosclerotic plaques [11].

1.3 Atherosclerosis

One of the most common conditions that affect the circulatory system and in particular the arteries, is arteriosclerosis. This condition results from the accumulation of fibrous connective tissue at the expense of the elastic component. Atherosclerosis, a specific type of arteriosclerosis brought on by the accumulation of fatty plaques, cholesterol, and other chemicals in and on the artery walls, is the process that gradually restricts blood flow to one's organs and tissues and can result in serious health hazards. Smoking, eating poorly, and several genetic factors are all potential causes [12]. Any rupture of the plaque itself, which is

often protected by an endothelial layer and a thin fibrous cap, can result in thrombosis and total obliteration of the vessel lumen, which will stop the flow of blood. This condition is the primary cause of death and is responsible for 60% of cerebral strokes and 90% of coronary events. Additionally, 30% of cases of dementia and the majority of cases of peripheral artery disease and heart failure are caused by atherosclerosis [13]. The severity of the pathology is also given by the fact that once it has developed, atherosclerosis looks to be an unstoppable process with the potential for ongoing growth. As long as it does not impair the blood flow within the arteries, atherosclerosis generally does not result in symptoms. Depending on whether atherosclerosis is localized in the coronary area (angina, myocardial infarction), cerebral (stroke or TIA), intestinal, renal, or peripheral areas, ischemia and heart attack symptoms will vary. In particular, the first symptoms of a carotid obstruction may only become evident when it becomes severe enough to deprive the brain of blood, causing a stroke or transient ischemic attack. In the absence of symptoms, however, technologies such as echo doppler and CT-Angio are reliable in highlighting the presence of lesions [14].

1.3.1 Atherosclerotic plaques

Atheroma, better known as atherosclerotic plaque, can be defined as a degeneration of the arterial walls due to the deposit of plaques formed essentially by fat and scar tissue. Large and medium arteries, which are predominately made of elastic tissue (particularly in the large arteries), are the principal sites of atherosclerotic lesions. Additionally, they frequently appear in areas that are prone to their development, such as the spots where arteries split off and a turbulent blood flow is present. The atherosclerosis process starts extremely early, in early adulthood or adolescence (childhood obesity problem). Figure 8 shows the different stages of progress of an atherioschelorite plaque inside a blood vessel. As can be observed, plaque formation only happens at the end of the atherosclerosis process, making it impossible to detect the disease when it first manifests. The atherosclerotic plaque is characterized by a confined thickening that can range in size from a few millimeters to a few centimeters, is whitish or slightly yellowish in color, has a firm consistency, and has a continuous surface that can be smooth or rough.

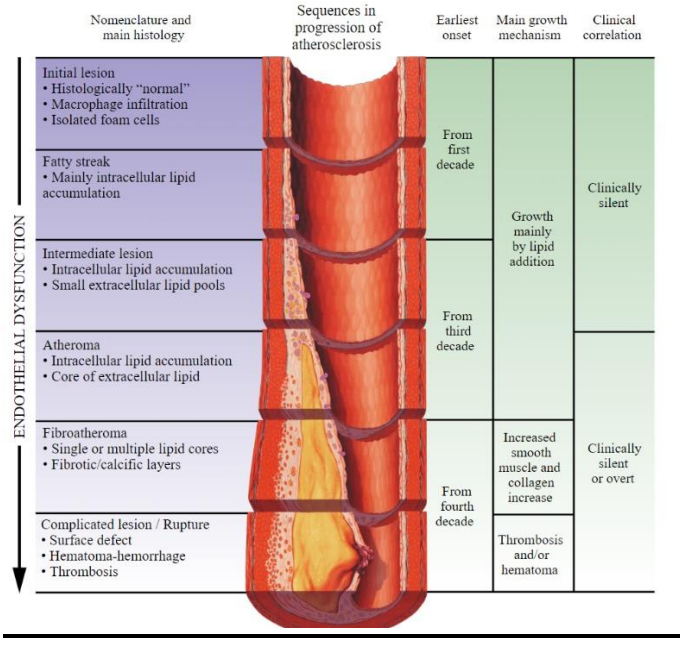

Figure 8. A progressive sequence of an atherosclerotic plaque. Atherosclerotic plaques form externally during the first phase of training; the vase takes on an ovoid shape while the transversal section usually maintains a circular shape [15].

The danger of the carotid plaque is not represented only by the reduction of blood flow to the brain. When a piece of the carotid plaque breaks off, the small plug travels to the brain and obstructs a cerebral artery, causing thrombosis or embolism, which are both very serious acute complications.

1.4 Wall shear stress

The wall shear stress (WSS) is one of the most treated and studied parameter in the literature in association with the presence of atherosclerotic plaque. The Wall Shear Stress, by definition, is the product between Wall Shear Rate (WSR) and blood viscosity and represents the force that the blood flow exerts tangentially to the arterial walls. On the other hand, the shear stress expresses the kinetic energy lost by the blood as it moved along the arterial wall and offers a measure of the mechanical stimulus that the endothelium received. If we indicate the distance between two moving fluid layers with ∂r and the difference between the relative speeds of movement with ∂u, the relative shear rate is indicated by the ∂u/∂r ratio. The primary factor affecting the shear stress is the wall shear rate, which is determined by calculating the gradient of erythrocyte velocity with respect to the artery radius close to the vessel walls:

$$WSR = \frac{\partial u}{\partial r}$$

For Wall Shear Stress (τ), on the other hand, we indicate the product of the blood viscosity (μ) for the Wall Shear Rate:

$$\tau = \mu \cdot WSR$$

For Newtonian fluids, for which the shear stress is directly proportional to the shear rate (constant viscosity), shear stress (Kg$\cdot m^{-1} \cdot s^{-2}$) can be calculated starting from the viscosity μ of the fluid under examination and the shear rate (s^{-1}) according to the following formula:

$$\tau = \mu \cdot \frac{\partial u}{\partial r}$$

By definition, a curve passing through the origin that has the viscosity as its angular coefficient can be used to represent the relationship between shear stress and shear rate as shown in figure 9.

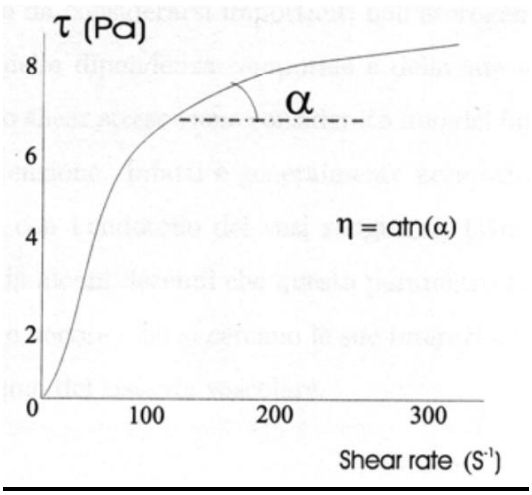

Figure 9. Trend of shear stress as a function of shear rate [16].

1.5 Blood

As seen, also the properties of the fluid are very important for the study of the wall shear stress. That of our interest, blood, is a fluid tissue found in all animals with a circulatory system. First and foremost, it transports oxygen and nutrients to the body's cells while simultaneously removing carbon dioxide and other metabolites from them. Variations in viscosity can occur in blood because it is a complex fluid made up of suspended particles in liquid phase (plasma). As shown in figure 10, the suspended particles represent about 46% of the total blood volume [17].

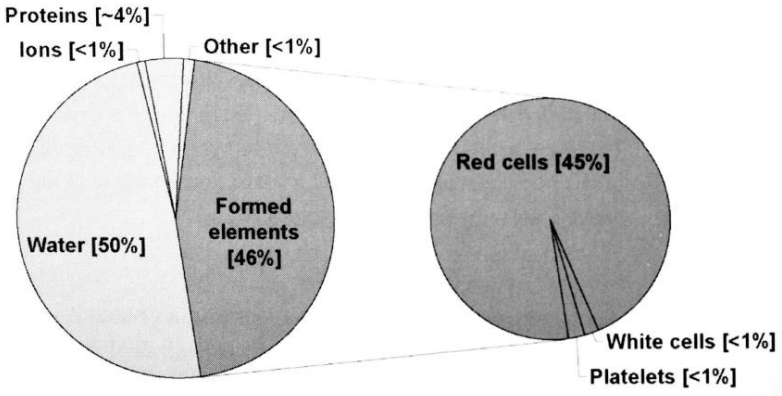

Figure 10. Blood composition [17].

For low values of shear stress, the blood behaves like a non-Newtonian fluid. In this case, the formation of aggregates of red blood cells (rouleaux) and therefore the viscosity is no longer constant, but increases as the rate of shear decrease (Figure 11). The model that best describes the viscous behavior of blood is that of Casson:

$$\sqrt{\tau} = \sqrt{\tau c} + \sqrt{\mu \frac{\partial u}{\partial r}} \qquad \text{for } \tau \geq \tau c$$

$$\frac{\partial u}{\partial r} = 0 \qquad \text{for } \tau < \tau c$$

For $\tau < \tau c$, the blood behaves like a solid, because of extensive rouleaux formation. The viscosity also depends on temperature and hematocrit (percentage of suspended cells in the blood volume). For a hemacrotic of 45% and a temperature of 37° C a standard value of $4 \cdot 10^{-3}$ Kg$\cdot m^{-1} \cdot s^{-1}$ is used.

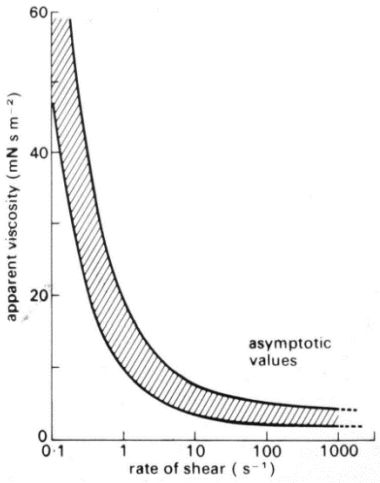

Figure 11. Viscosity trend as a function of the shear rate [16].

It can therefore be said that the behavior of blood in the human body as a whole is of a non-Newtonian type, for large values of shear rate ($\frac{\partial \mathrm{u}}{\partial \mathrm{r}} > 100\ S^{-1}$) on the other hand, can be considered as Newtonian.

Chapter 2- Methods

2.1 Computational fluid-dynamics

It is possible to solve and analyze fluid dynamics issues using a computer by using the computational fluid dynamics (CFD) method. With the help of computational fluid dynamics (CFD), it is possible to solve the Navier-Stokes equations, or their approximations, i.e. the fundamental equation used to describe the fluid flow.

In this thesis, numerical simulations are performed, through the use of the Ansys Fluent software to solve problems of interest, in particular mathematical models, using the method of finite volumes. The mathematical model consists of a set of governing equations, defined on a domain, with appropriate boundary conditions. The Ansys fluent solves the laws governing the fluid dynamics on the basis of the CFD method, converting the governing equations into algebraic equations.

Three laws govern how fluids flow: the laws of conservation of mass, momentum, and energy. However, if the fluid under consideration is incompressible (a fluid with costant density), the energy law can be ignored. There are two ways to express these laws: by means of differential or integral equations. The local fluid and flow behaviour is described by differential equations, while the integral form analyzes the behavior of finite quantities of the fluid within a control volume. They are as follows:

	Mass conservation law:	**Momentum conservation law:**
Differential form	$\nabla \cdot \boldsymbol{v} = 0$	$\rho\,(\boldsymbol{v}\,\nabla)\boldsymbol{v} = -\nabla p + \mu\nabla^2\boldsymbol{v}$
Integral form	$\int_{S_0} \boldsymbol{v} \cdot \boldsymbol{n}\, dS = 0$	$\int \rho \boldsymbol{v}(\boldsymbol{v} \cdot \boldsymbol{n}) dS = -\int pn\, dS + F_{visc}$

Table 1. Conservation laws in differential and integral form. The laws governing the flow of a fluid.

where:

- $\boldsymbol{v}$ is the velocity vector;
- ∇ is the gradient;
- $\nabla \cdot \boldsymbol{v}$ is the divergence of the velocity vector;
- ρ is the density;
- p is the pressure;
- ∇p is the pressure gradient;
- μ is the viscosity coefficent;
- $\boldsymbol{n}$ is the normal versor;
- S is the surface;
- F_{visc} is the viscous force

The Navier-Stokes equation can be expressed in the following dimensionless form:

$$\frac{\partial \boldsymbol{v}^*}{\partial \mathrm{t}^*} + (\boldsymbol{v}^* \cdot \nabla^*)\, \boldsymbol{v}^* = -\nabla^* p^* + \frac{1}{Re}\nabla^2 \boldsymbol{v} + \mathbf{b}^*$$

• $\partial\, \boldsymbol{v}^*\, (\mathbf{x}^*, t^*)$ is the partial derivative of the flow velocity with respect to time, the velocity is defined as a function of both displacement and time.

• $(\nabla^*\, \boldsymbol{v}^*\, (\mathbf{x}^*, t^*))$ is the gradient of the velocity as a function of the displacement.

• $\boldsymbol{v}^*\, (\mathbf{x}^*, t^*)$ is the speed as a function of displacement and time.

• $-\nabla^*\, p^*\, (\mathbf{x}^*, t^*)$ is the pressure gradient as a function of displacement and time.

• Re is the Reynolds number, which measure the ratio between inertia and viscous forces, viscosity also influencing boundary layer dyanmics and diffusion phenomena. The Reynolds number at a channel with diameter D is given by the formula: $\frac{v\,D}{\nu}$ where v is the velocity and ν is the kinematic viscosity, which is the ratio among dynamic viscosity and density.

• $\nabla^2\boldsymbol{v}$ * ($\mathbf{x}$*, t*) is the Laplacian of velocity as a function of displacement and time.

• $\mathbf{b}$* ($\mathbf{x}$, t) is the volume action as a function of displacement and time

It is possible to derive this equation from both the law of conservation of momentum and the law of conservation of mass. This law is established under specific circumstances where the fluid is Newtonian and incompressible. Any fluid flow can be described by the Navier-Stokes equations, which also describe the macroscopic behavior of a moving fluid.

The main problem in solving the NS equations lies in the non-linearity of the convective terms which makes it difficult to find analytical's solutions.

2.1.1 Finite volume method

The software uses numerical methods by transforming the governing equations into algebraic equations, linearizing them.

Ansys numerically solves the governing equations using the finite volume method, which consists in dividing the fluid domain into small control volumes, called cells, through discretization. The governing equations, in integral form, are applied to each single cell, in this way we have a set of algebraic equations. In this instance, a finite volume in the flow domain is subjected to the fundamental laws of momentum and mass conservation. The problem's unknowns are primarily the velocity vector and the pressure, which are studied on specific cell locations known as nodes, which can be either the vertices or the cell centers. With this approach, the work is made easier because the unknowns are calculated at specific points rather than by searching for functions inside the cell. In the center of the cell, the conservation laws of mass and momentum are put into practice, algebraic equations are created that relate to the neighboring cells, and the two components of velocity and pressure are obtained. Then the non-linear problem is simplified by converting this system into a set of algebraic equations, easily solved by a computer.

The software, Ansys, performs the discretization process, and this can be fully explained through an example, considering a flow that occurs in a rectangular domain with two wall boundaries and two open boundaries. On a control volume, each individual cell is subject to the law of conservation of mass in integral form. The law of conservation of mass can be explicitly stated, the inlet mass is the same as the outgoing mass of the control volume because the fluid is incompressible and there is no mass accumulation.

Given the geometry shown in figure 12, it is clear that the flow is constant and moves positively in the abscissa-directed direction from left to right. The incoming and outgoing mass flows are equal, making the flow positive from left to right. It is possible to conclude from this observation that the input and output speeds are equal.

Figure 12. Representation of a rectangle divided into cells, represented by the blue squares

The domain is divided into cells while taking into account a stationary regime (the speed does not depend on time). By using a finite volume method with a centered cell, the equations' linearization process anticipates that the unknowns will be defined at the cell's center. The law of conservation of mass is first applied to each cell in integral form, balancing the inflows and outflows from each surface of the control volume, where the velocity is assumed to be the average of the velocities defined in the centers of the adjacent cells. The error (e1) results from this approximation.

In particular by analyzing the cells of any domain (Figure 13)

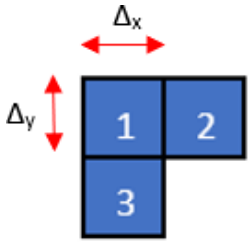

Figure 13. Cells enumaration.

The volumetric flow rate ($Q_{1\text{-}2}$) crosses the right face.

$$Q_{1\text{-}2} = u_{1\text{-}2}\Delta y + e1 \tag{1}$$

where the sides of the cell are represented by Δx and Δy. Through interpolation of the velocity values assumed in the center of cells 1 and 2, i.e. the average of the two speeds, the speed in the x direction is expressed, introducing a new error:

$$u_{1\text{-}2} = \frac{u1+u2}{2} + e1 \tag{2}$$

The flow is obtained through the other faces, respecting the boundary conditions. Substituting the equation(2) in (1), we obtain:

$$Q_{1\text{-}2} = \frac{u1+u2}{2}\Delta y \tag{3}$$

Finally, in the same way, to calculate the mass flow through face 1-2, it is necessary to interpolate the velocity of cell 1 and cell 2, in the y direction. Furthermore, the contribution of the top and left face is zero. The law of conservation of mass for cell 1 can be written in the following way:

$$\frac{\Delta y}{2}u1 + \frac{\Delta x}{2}u2 + \frac{\Delta y}{2}v1 + \frac{\Delta x}{2}v3 = v\Delta x\,\Delta y \tag{4}$$

This indicates that the mass or volume entering the control volume equals the amount of mass or volume leaving the control volume. Additionally, it implies that the mass leaving this volume or control cell will enter the cell next to it: there will not be any mass loss. This indicates that each control volume's mass conservation is assured. Additionally, the mass entering the control volume will equal the mass exiting the control volume.

This procedure can also be applied to the law of conservation of momentum, which however has non-linear terms. Given the integral form of the momentum equation:

$$\int \rho \boldsymbol{v}(\boldsymbol{v}\cdot\boldsymbol{n})dS = -\int pn\,dS + F_{visc} \tag{5}$$

The first term denotes the motion that exits the chosen control volume. The pressure force on the control surface is the second. The third force acting on the control surface is the viscous force. Since we have a velocity product and a velocity component, the first term is non-linear. The equation in this situation needs to be linearized. For instance, when determining the output momentum in the x direction between cells 1 and 2, we get the following results:

$$M_{x,1\text{-}2} = \rho u_{1\text{-}2}\, u_{1\text{-}2}\Delta y + e = \rho \frac{(u1+u2)^2}{2}\Delta y + e1 + e2 \tag{6}$$

where, $M_{x,1\text{-}2,}$ is the momentum of flow in the x direction.

The non-linear therms $u1^2$, $u2^2$ and u1u2 are linearized as follows:

$$u = u_{assumed} + \Delta u \tag{7}$$

The velocity variable u is expressed with a hypothesized value plus a correction of that value.

If we have a function of u, it can be developed in Taylor series:

$$f(u) = f(u_{assumed} + \Delta u) = f(u_{assumed}) + \Delta u f'(u_{assumed}) + \frac{\Delta u^2}{2} f'' + error \tag{8}$$

If we consider, for example, the quadratic function:

$$f(u) = u^2,\ f(u_{assumed}) = u_{assumed}^2,\ f'(u) = 2u \text{ and } f'(u_{assumed}) = 2u_{assumed}$$

and inserting it again in the Taylor series, we obtain:

$$u^2 = u_{assumed}^2 + \Delta u 2 u_{assumed} + \text{linearization error} \tag{9}$$

This process is applied to all non-linear terms of the balance equations, which is then solved iteratively, that is, the attempted solution is updated each time with the calculated value Δu, up upon reaching an acceptable linearization error.

2.1.2 Linearization and discretization error

Linearization and discretization errors were introduced into the process described. The former results from the linearization of the equations, where a value is assumed and the process is repeated numerous times until a result is obtained with a minimum amount of error by setting a tolerance value. When the mass and momentum imbalances are below some established tolerances, the iterative process comes to an end. The discretization of conservation laws in algebraic equations yields the latter error. There are two ways to reduce the error: The first determines a larger number of cells in the domain to enhance the mesh quality; the second determines a larger number of nodes for each cell to enhance the accuracy of the interpolation. The construction of the mesh must be carefully considered because, as must be noted, reducing one type error can increase the other.

2.2 Definition of the problem

The geometrical model was downloaded from the Grabcad community website and then uploaded to Ansys Fluent.

The geometry has been uploaded to Ansys Fluent and is shown in figure 14. The diameter internal carotid artery (named outlet1) is around 4.5 mm, the diameter of external carotid artery (named outlet2) is around 3.0 mm and the diameter of the common carotid artery(named inlet) around 6 mm.

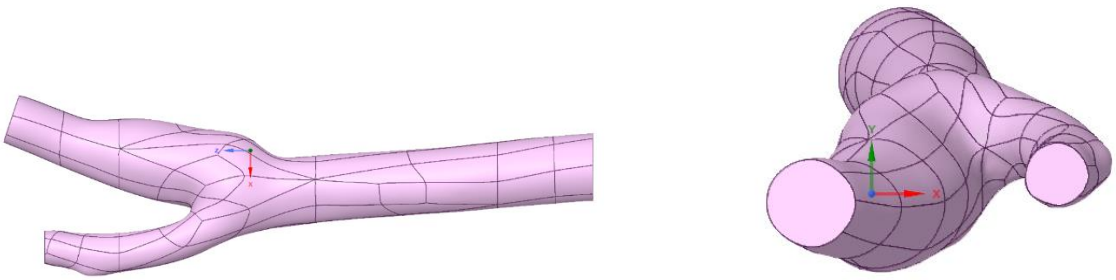

Figure 14. Z-X and Y-X views of the right carotid artery. The carotid sinus is the enlargement that is visible between the common carotid artery's termination and the start of the internal carotid artery.

The same geometry was employed for the study of the flow in the presence of atheroschloric plaques, with the addition of plaques in the carotid sinus region.

Adding obstructions

Since ovoid structures most closely resemble those found in the real-life situations, the obstructions, which are the arteriosclerotic plates, have been modeled as such, as shown in figure 15.

The dimensions have been chosen consistently with what is reported in the literature [15]. We chose a major axis of 8 mm, which represents the length of the plate, and a minor axis of 6 mm, which represents the thickness ,and, when fused to the geometry already present, will become about 3 mm.

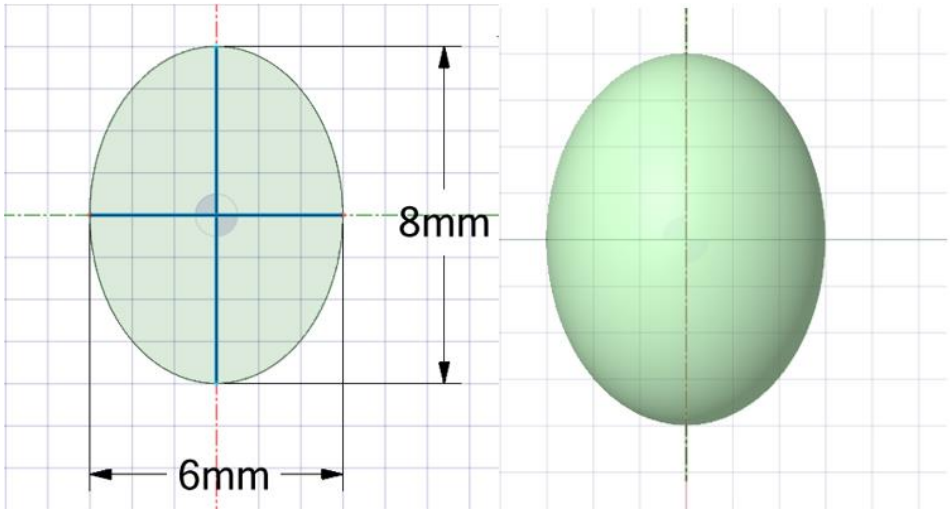

Figure 15. Ovoid plate profile, with the 3D version on the right and the 2D version on the left.

After the geometry was created, it was necessary to: Use the “merge faces” command in the “repair” control panel, to merge the faces on the geometry in the area of interest. This region, into which the occlusion will be inserted later, must be at least as large as the entire occlusion. The occlusion was then relocated to the area of interest, aligning its main axis with the model's walls. Following completion of this, the "combine" command was used in the "design" panel. By using this command, we could combine the two geometries into one single body. Utilizing the “pull” command, which is always present in the design, was the final step. This command caused the plate to be pushed down of an additional 0.15 mm. By translating the newly created geometry, it was then possible to change the occlusion level symmetrically as a result of this command. Figure 16 shows the artery with the maximum degree of obstruction, The diameter of these occlusions was then reduced by 1 and 2 mm respectively, to then obtain the two new geometries shown in figure 17.

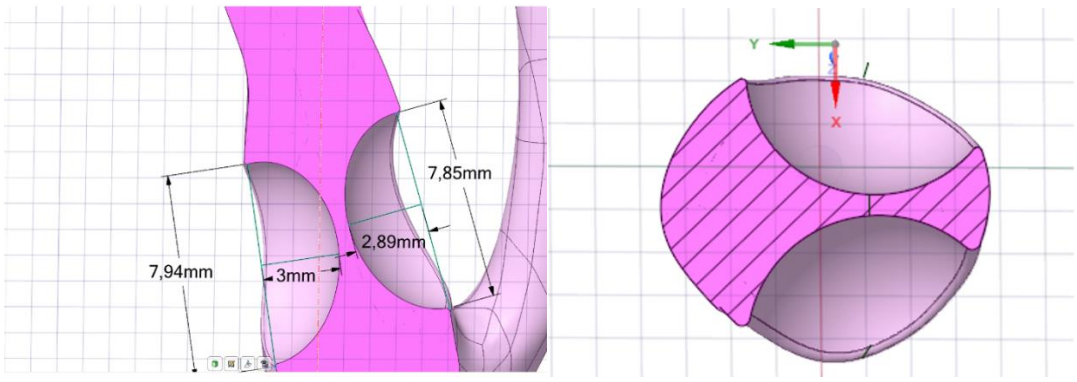

Figure 16. Sections of the carotid artery with the maximum degree of obstruction

It is evident that the two plates do not have “perfect” symmetry, especially due to the irregular geometry of the domain. For the purposes of this thesis, this is a negligible issue because such plates are never symmetrical in real-world situations.

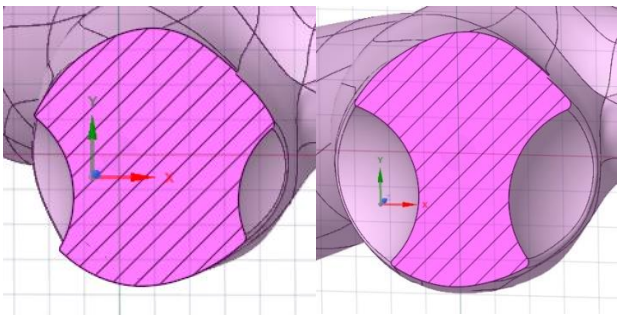

Figure 17. On the left, the geometry with the plates with a thickness of 1mm, on the right, the geometry with the plates with a thickness of 2mm

Although the only parameter that changed was the diameter, the length of the occlusion also decreased as the diameter decreased. The geometries studied will therefore be the healthy one, where there is no presence of plates, the one with the maximum degree of obstruction, in which the diameter of the plates is about 3-mm, and the other two instead have respectively plates with a diameter of 2-mm and 1-mm, as shown in figure 17.

2.3 Meshing

In the second phase of the work the mesh was generated. The geometry determined in the previous step is imported into the “Mesh” section of the software, where two different types of “Face sizing” are applied: Through this option, the size of the cells and the type of mesh are assigned. With reference to Figure 18, it should be noted that the mesh used in the domain is triangular and the size of the cells is 0.1 mm. The same process was used for the second "face sizing," but this time the "sphere of influence" command was added, allowing us to choose a circular area in which to apply a particular mesh. The 1.2 cm-diameter sphere is centered in the region of the bifurcation. We chose a mesh with a dimension of 0.5 mm, always of the triangular type, because we want to fine-tune the mesh in this region, where the changes are more pronounced.

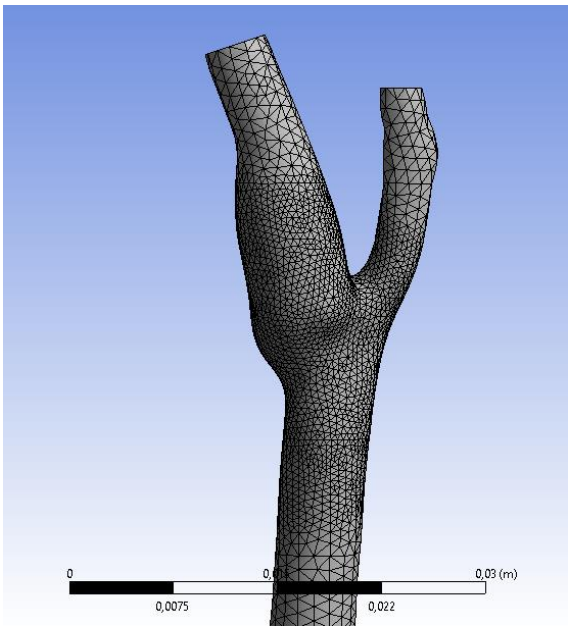

Figure 18. Mesh geometry. The “sphere of influence” command, as seen, has caused the size of the cells in the bifurcation area to decrease.

Finally, the "inflation" command was employed, allowing us to build layers close to the domain wall as shown in the following figure. Due to the no-slip boundary condition, changes near the walls are typically more abrupt, allowing us to sweat them more effectively. A growth rate of 1.2 and a thickness of 0.6 mm was chosen for 4 layers, the resultant mesh is shown in figure 19.

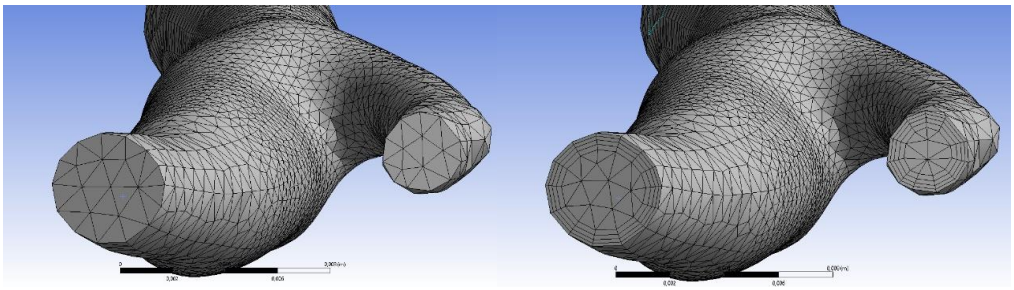

Figure 19. In the right image the mesh with no “inflation” command and left mesh with “inflation”

Name selection

This phase consists of giving names to various domain components. The software is actually able to automatically assign the type of condition to the contour that will be applied, making this assignment very crucial as it will also affect the subsequent steps. With reference to figure 20 we can observe the areas wall_outle1, wall_outlet2 and wall_bifurcation. These areas have been selected, as they can be analyzed individually in the following steps in the CFD-postprocessing. The rest of the arterial wall, with the exception of those previously selected, was named wall_rest, therefore always of the “wall” type. The inlet, on the other hand, coincides with the entrance of the common carotid artery, Outlet 1 with the exit of the internal carotid and outlet 2 with the exit of the external carotid artery.

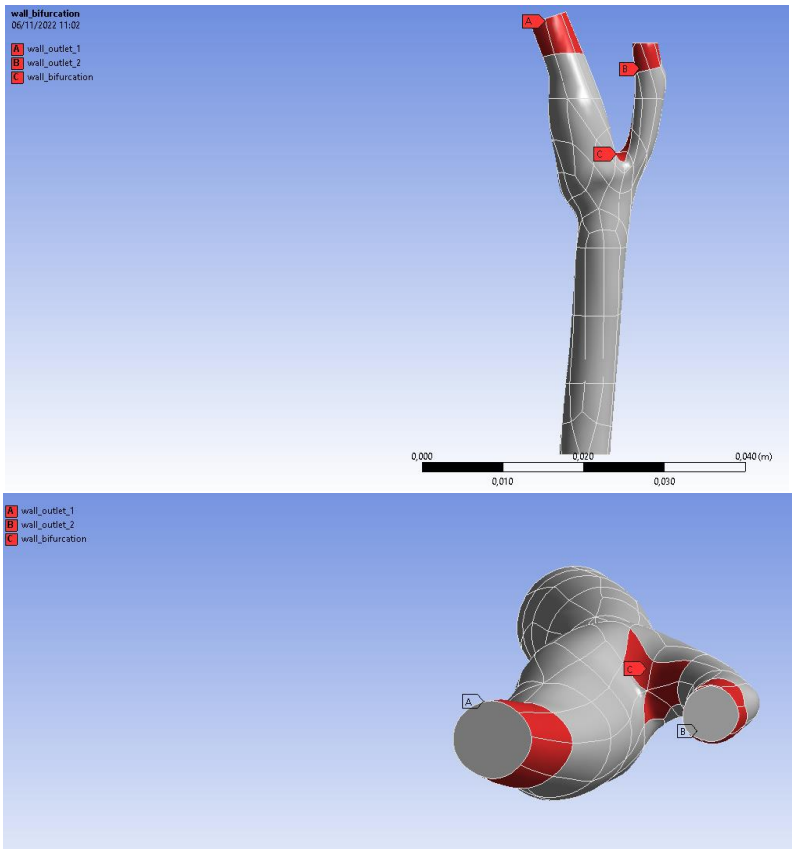

Figure 20. Display of wall_outle1,wall_outlet2 and wall bifurcation (in red).

The walls related to the outlets have been selected in order to study how the WSS varies downstream of the obstruction. The bifurcation area instead, because it was proved to be the area subject to the highest WSS value during the cardiac cycle.

2.4 Numerical modeling

Fluid dynamics simulations with Ansys Fluent:

The numerical tests were carried out using the Ansys Fluent 19.2 software. In this phase, the conditions that express the physics of the system to be analyzed are imposed. The general activities page, shown in Figure 21, allows you to configure some generic settings. In the “Type” command “Pressure-Based” was chosen, which enables the Navier-Stokes solution algorithm based on pressure. This approach was developed for low-speed incompressible flows. With reference to Figure 21, from the setup menu, you can set a static, “steady” or dynamic, “transient” type of test. The first refers to the resolution of a constant flow over time, while the second refers to a time-dependent solution. In the case under analysis, the transient type was used as the input velocity is not constant over time.

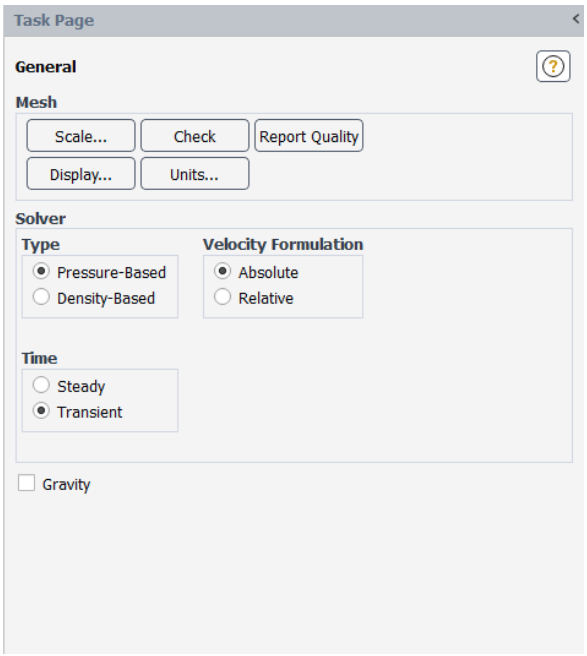

Figure 21. Option to define a stationary or transient simulation.

Subsequently in the "model", figure 22, the flow was assumed to be laminar. This because in large vessels, the flow is for the most part of this type, that is, the fluid particles flow linearly one above the other. In addition, thanks to the selection of laminar, it is possible to set the viscosity of the blood as a variable, in particular to set it as a function of the wall shear.

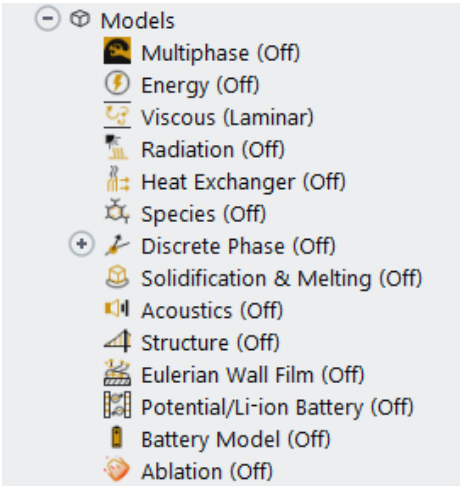

Figure 22. Model type option selected, laminar.

Subsequently, in “Materials” the type of material treated was chosen, between fluid and solid. Having chosen the fluid material, defined with the name “blood”, it was assigned a density value of 1060 Kg /m^3. The viscosity, on the other hand, was modeled as a variable.

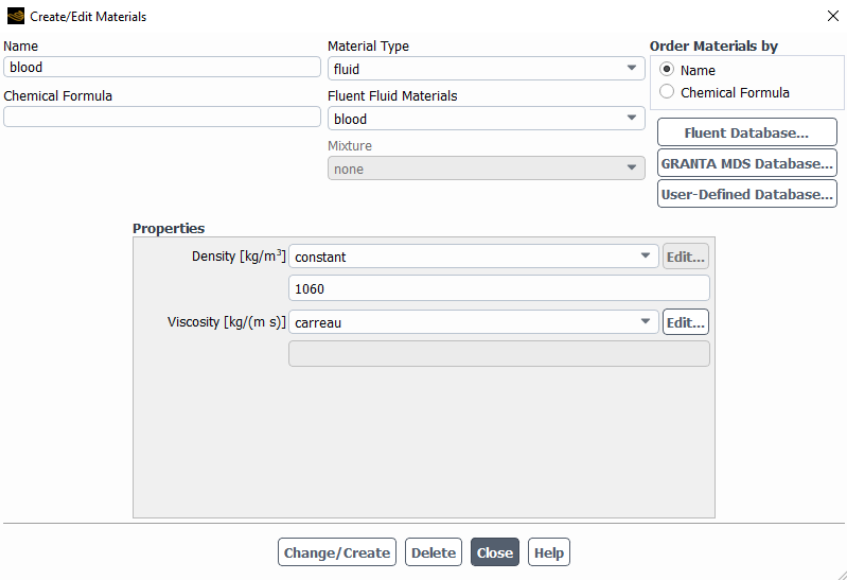

Figura 23. Panel for defining fluid density and viscosity.

The “carreau” model was selected for viscosity. Figure 24 also shows the values used in the simulations. [18].

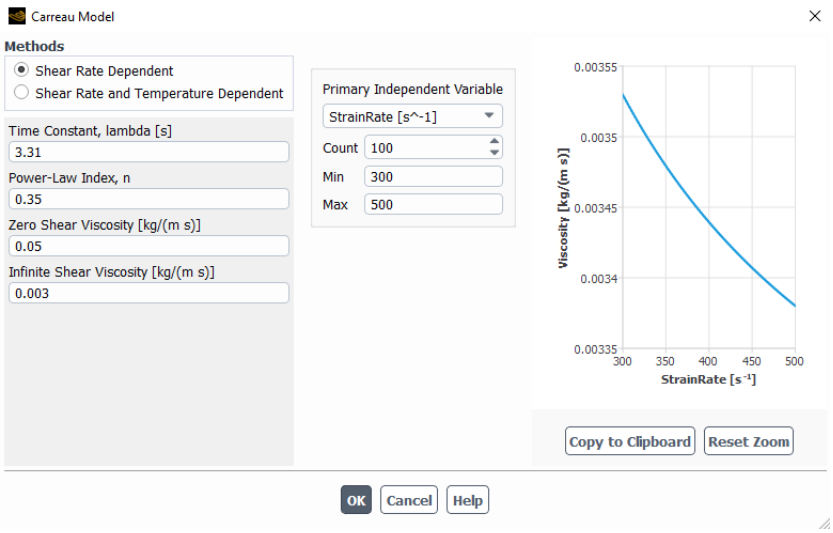

Figura 24. Carreau model panel.

where:

-Zero shear stress Viscosity (μ0) is the viscosity of a material when it is effectively at rest

-Time constant (λ)

-Infinite shear viscosity (μinf) is the viscosity that the fluid has at very hight shear rate

-Power law index (n) describes the rheology of the fluid where for Newtonian fluids n = 1 and n ≠ 1 represents non-Newtonian fluids

The speed entering the system, so entering the common carotid artery (inlet) was assigned as the input value. Figure 25 shows the mean velocity measured in the common carotid artery, used in this simulation [19].

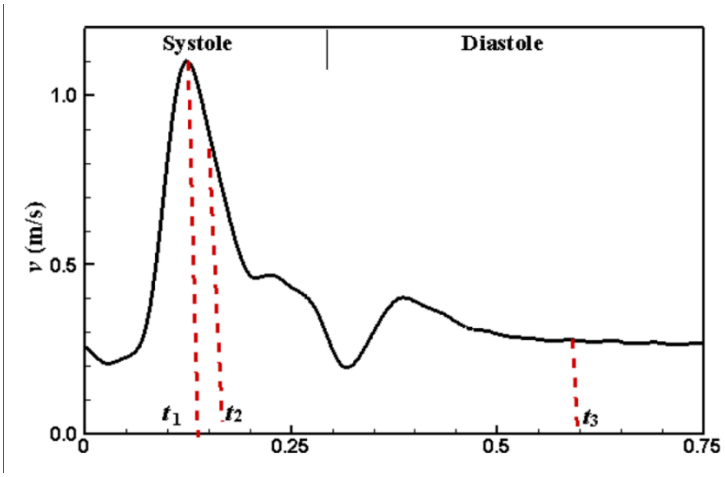

Figure 25. Profile of the blood velocity during the two phases, systole and diastole. We can observe t1, time of maximum systolic speed, t2 decreasing phase and t3 stationary phase [17].

The curve was discretized before being loaded into Ansys as a file, 75 points were selected from the curve at an interval of 0.01 s from each other, thus creating a table that can be loaded into Ansys. For the simulations, 2 cardiac cycles were used, the table was then duplicated, this because anomalous peaks were found at the beginning of the simulation of the first cycle, which instead disappeared in the second.

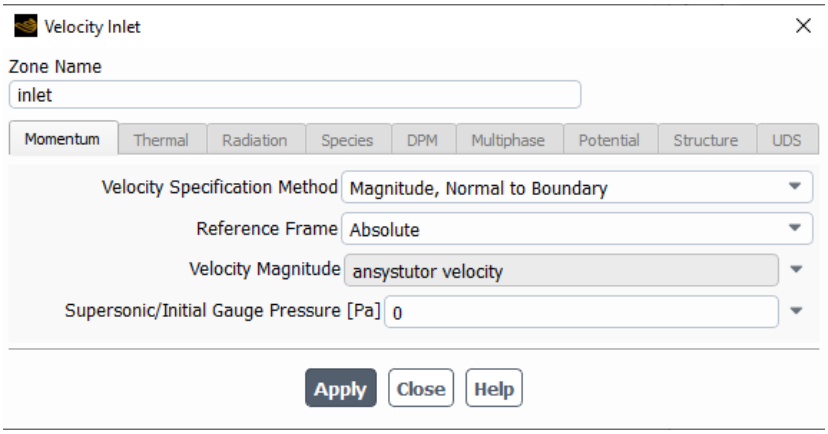

Figure 26. Loading the velocity profile into the system inlet which corresponds to the common carotid artery.

Then values were assigned to the pressure type outputs.

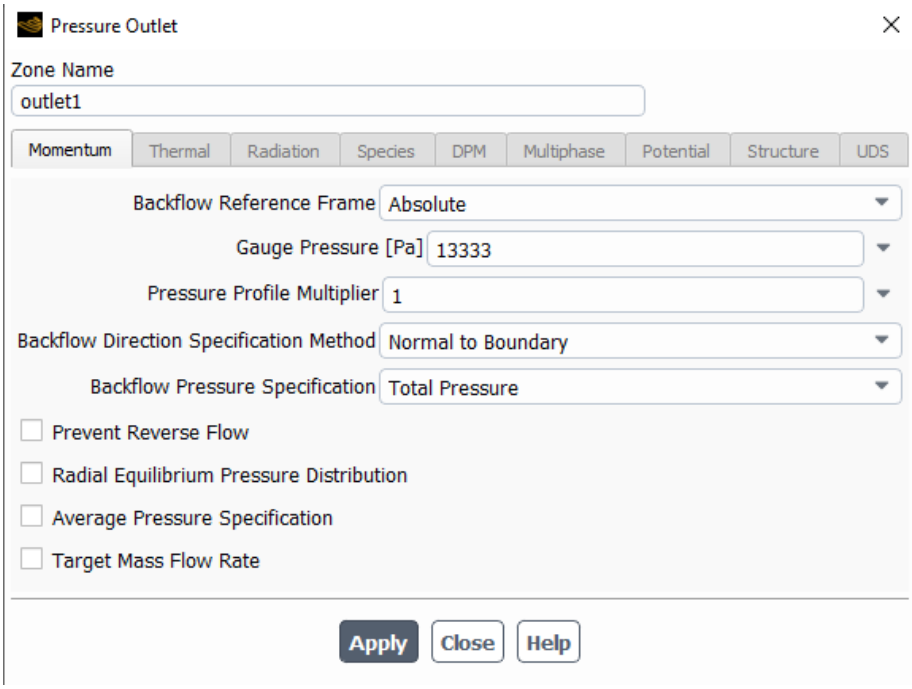

Figure 27. Assigning constant pressure to outlet1, which corresponds to the internal carotid artery.

The same pressure value was then assigned to the outlet 2. These values were chosen by placing an average between the standard blood pressure values of systole and diastole, or respectively of 80 mmHg and 120 mmHg, whose average, 100 mmHg corresponds to 13333 Pa.

The simulations were then initialized with hybrid initialization.

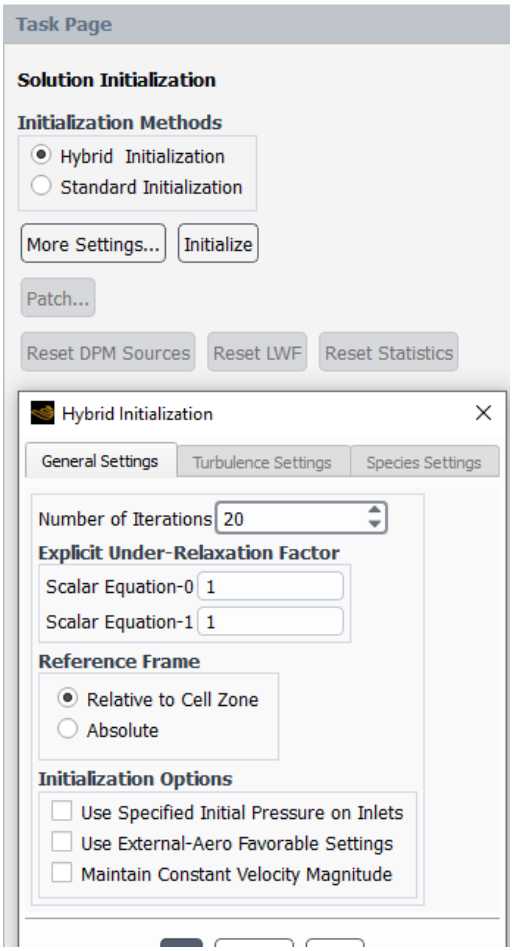

Figure 28. Hybrid initialization

The hybrid type was chosen because unlike the standard one, which just fills the properties with constant values, the hybrid one solves a number of iterations of a simplified equation system and thereby usually gets a better guess for the flow variables, in particular for the pressure field.

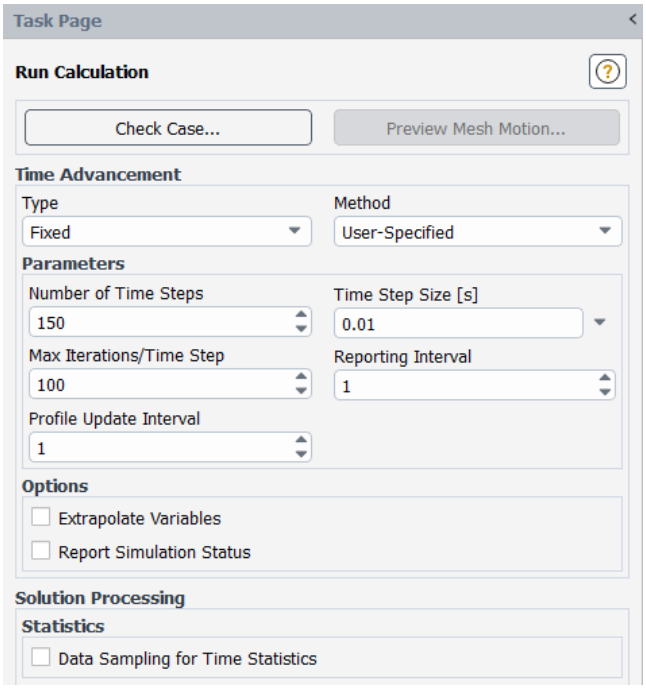

Figure 29. Dynamic simulation solution calculation settings.

The simulations are run for a number of time steps of 150, with a time step size of 0.01s, and a total time of 1.5s.

The maximum pressure values at the base of the internal, external and common carotid artery were then extrapolated in the CFD-postprocessing. The maximum was taken because it was not possible to extrapolate the mean from these locations. Even by inserting a modeled plane in the area of interest, the average values were obtained not considering the new model of the plane created, but the pre-existing one, making it impossible to extract them in a single portion of geometry. Therefore, in order to extract the maximum pressure values, dense series of points have been inserted in the areas of interest as shown in the figure 30, thanks to the point cloud command present in the CFD-postprocessing. Pressure gradient and resistance were calculated as follows:

$$\Delta P1 = P1 - Pout1 \quad (10)$$

$$\Delta P2 = P1 - Pout2 \quad (11)$$

$$\Delta P3 = Pin - Psin \quad (12)$$

$$R1 = \frac{\Delta P1}{Q1} \quad (13)$$

$$R3 = \frac{\Delta P2}{Q2} \quad (14)$$

$$R3 = \frac{\Delta P3}{Qsin} \quad (15)$$

The flows, instead, were calculated as follows:

$$Q1=V1mean*Areaoutlet1 \quad (16)$$

$$Q2=V2mean*Areaoutlet2 \quad (17)$$

$$Qsin=Vsinmean*Areasin \quad (18)$$

The main parameters used for the study are shown in the following figure.

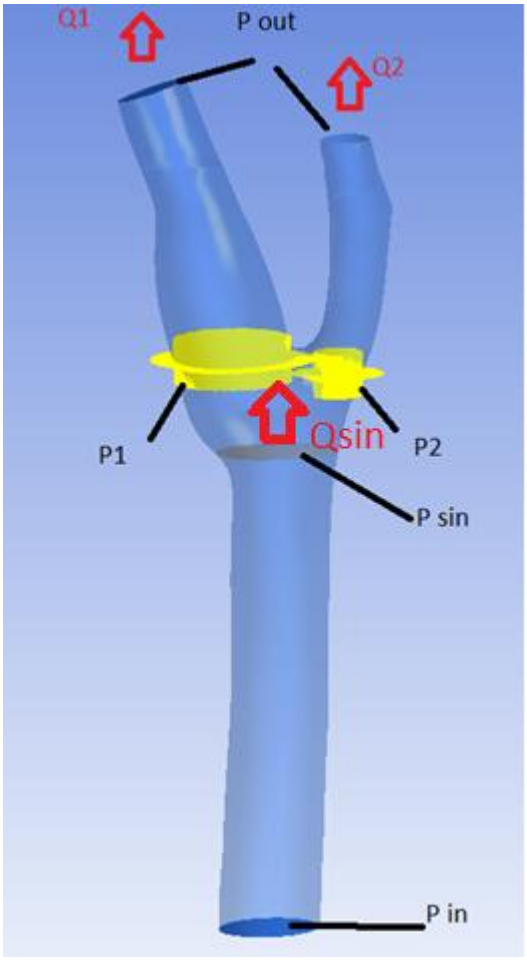

Figure 30. Main parameters used for the resistance calculations.

Chapter 3-Results

The last step is to analyze the data obtained from previous simulations. This last step is called CFD-postprocessing. Wall shear stress, velocities and resistance are the main analyzed values. These are evaluated both individually and then in comparison with the healthy case, i.e. bifurcation without occlusion.

3.1 Healty bifurcation

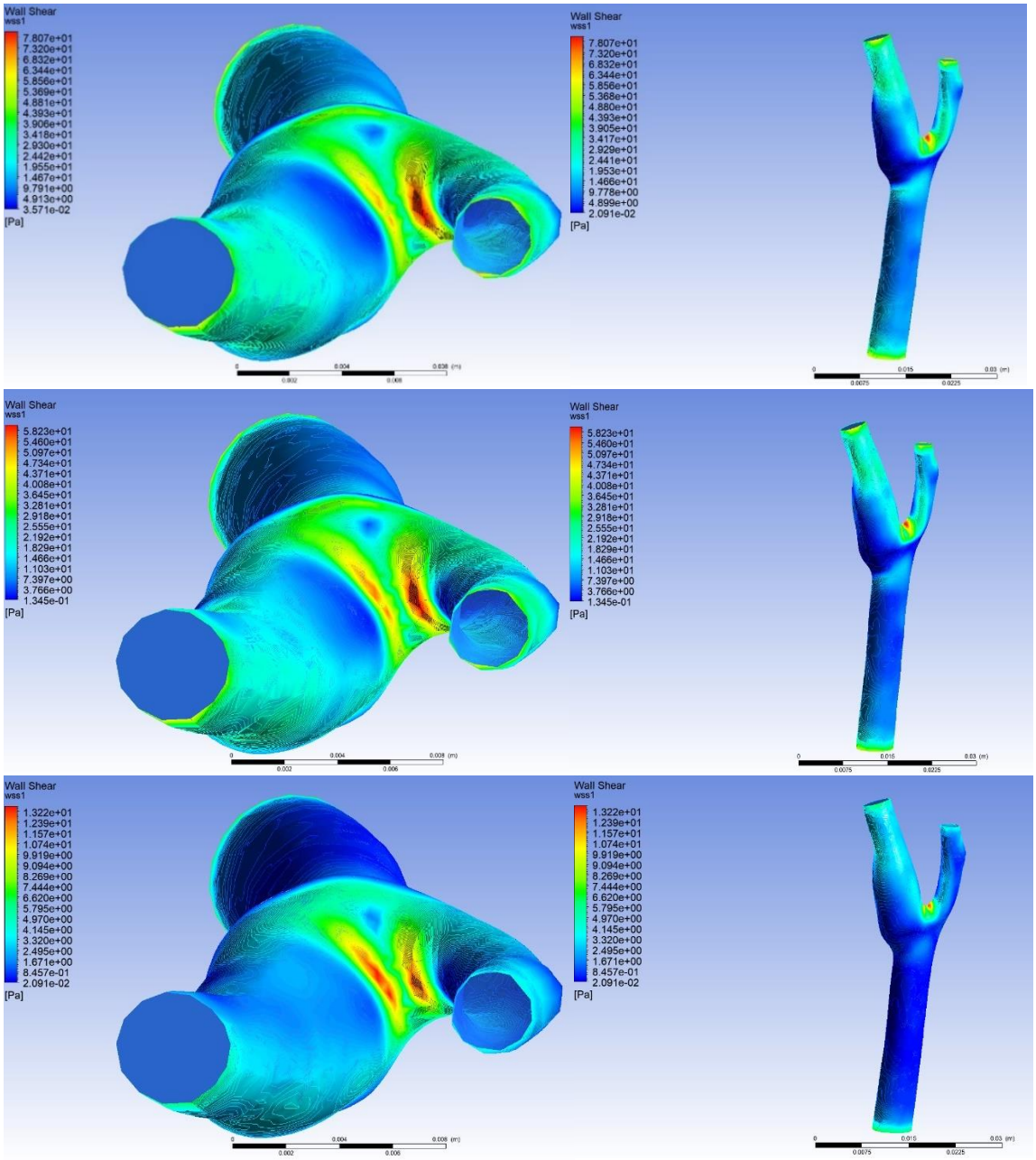

Figure 31. Representation of the WSS. Respectively in the first line the WSS at 0.13 seconds, in the second line at 0.16 seconds and in the third line at 0.31 s

The times of greatest interest have been chosen according to the velocity curve. Reference times are: a) that of maximum speed, corresponding to 0.13 s, b) time in the speed reduction phase, at 0.16s and c) the minimum speed time at 0.31s.

As we can observe from the upper figure 31 the maximum wall shear stress values, which precisely occur when the speed is maximum, are found in the area of the bifurcation, in particular adjacent to the internal carotid artery, and is about 78 Pa. At the same time, we can observe how the lowest values are found instead in the area of the carotid sinus. As the speed decreases, the maximum WSS values are found in correspondence with the internal carotid artery, as well as at the bifurcation.

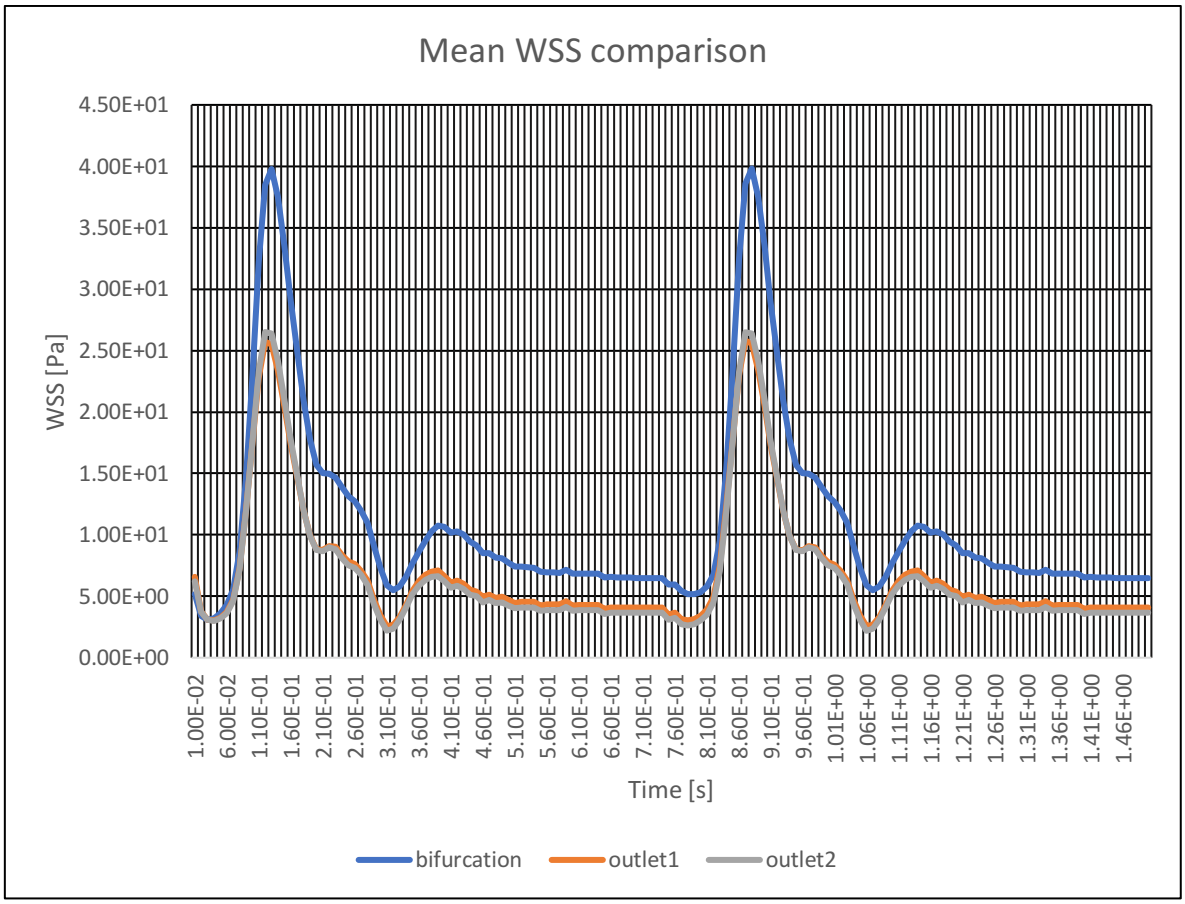

Figure 32. Mean WSS comparison between those of the wall_bifurcation (blue), wall_outlet1 (orange) and wall_outlet2 (grey).

Figure 32 shows that the WSS values at the bifurcation are significantly higher than those in the 2 outlets, especially for the peak of the systolic phase. Even if they have small differences, the values of the two outlets are comparable.

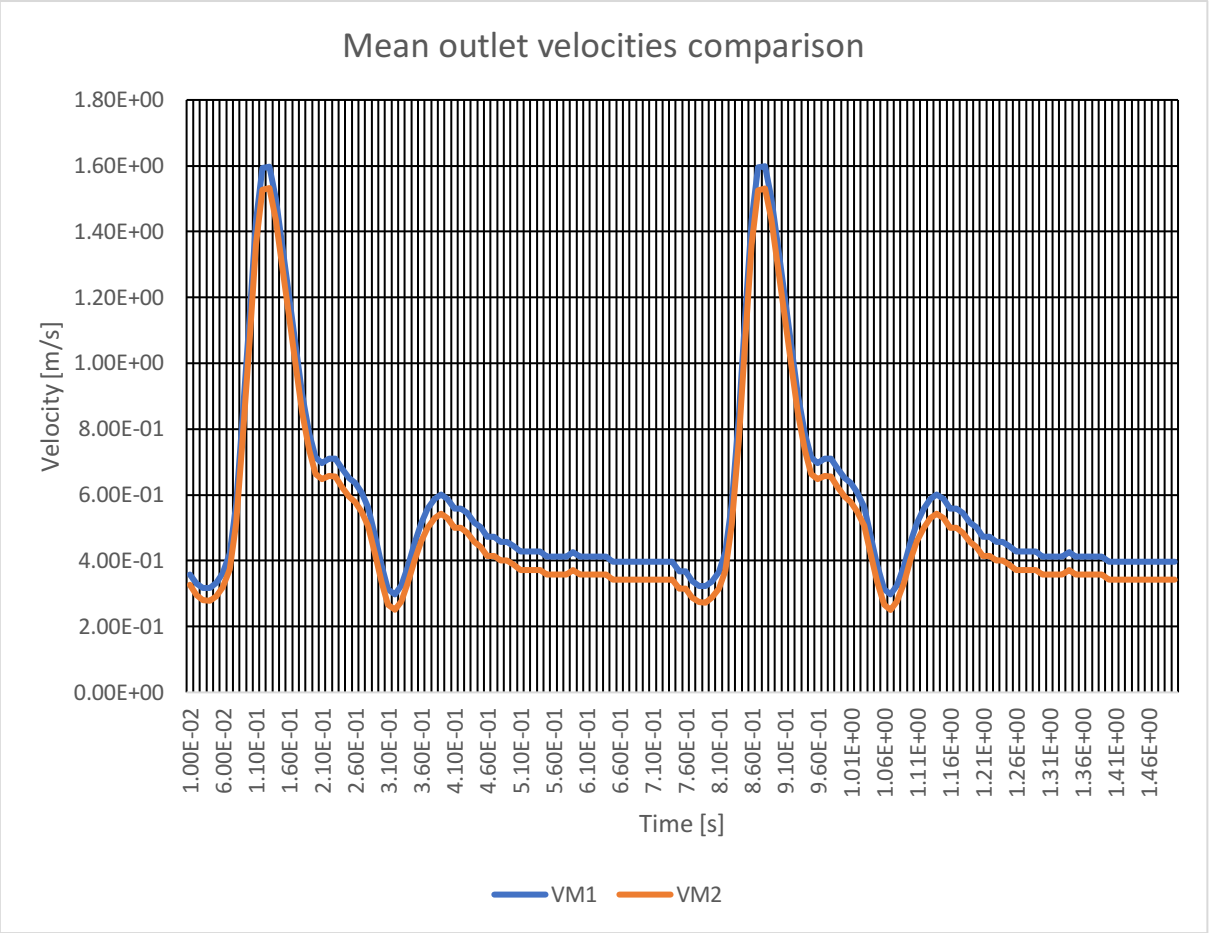

Figure 33. Comparison of the average speeds between outlet 1 (blue) and outlet 2 (orange).

Figure 33 shows that the mean velocity of the internal artery (outlet1) is greater, for thewhole cycle, than that of the external artery (outlet2).

In the following figures, a frontal plane to the artery has been chosen, in particular the one where the plaques are present, to see how the velocity profile varies according to the occlusion

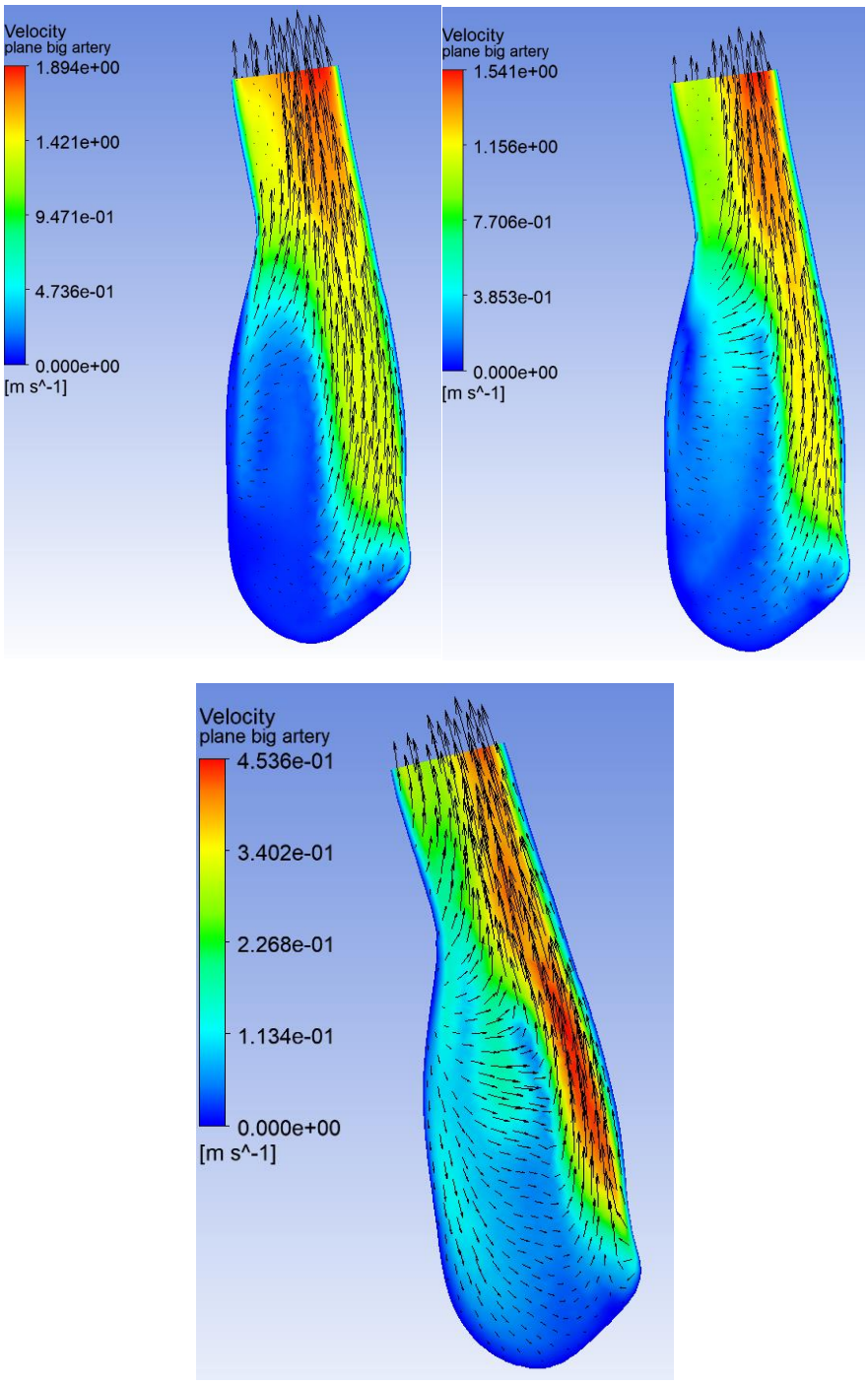

Figure 34. Color map and vector plot of the local velocity. On the top left,0.13s, top right,0.16 and bottom instead 0.31s

As we can see from the upper figure (figure 34), in the area of the carotid sinus there is a recirculation of the flow. At instants 0.13s and 0.16s, the maximum speed is found at the extremity of the outlet1, this does not

seem to be well centered but seems more thickened in correspondence with the wall opposite the swelling of the carotid sinus. At time 0.31s instead, the contribution of the carotid sinus becomes even more significant, in fact, the maximum velocity is found precisely in this area, suggesting that the recoil velocities actively act in the velocity flux especially in the diastolic phase.

The resistances are shown in the following graphs:

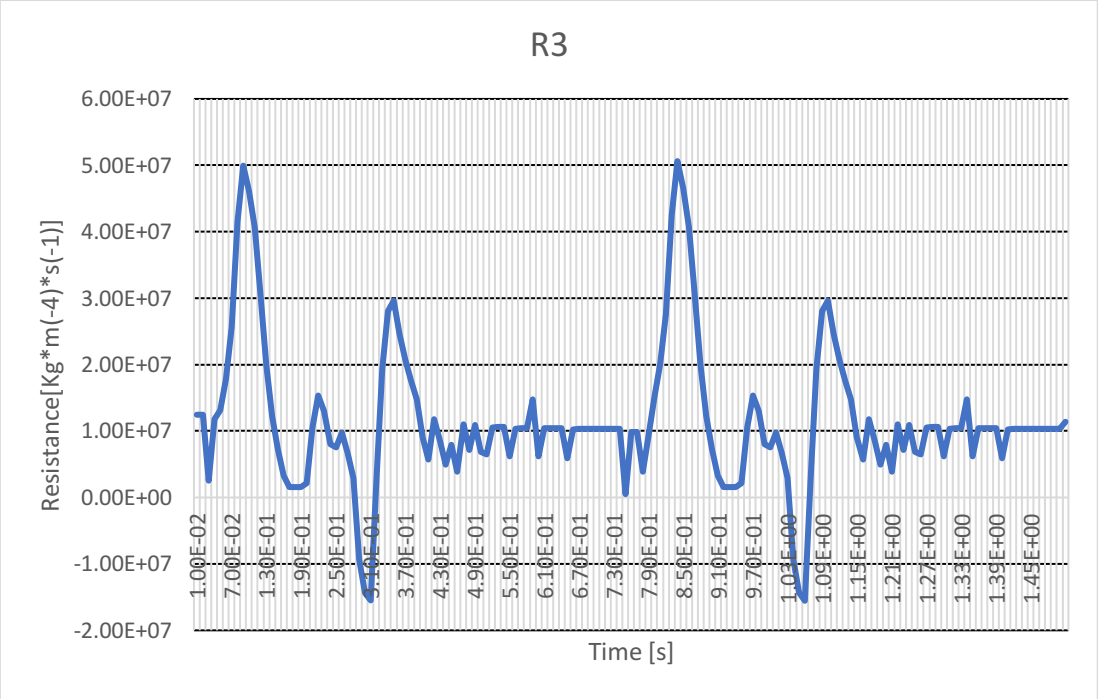

Figure 35. Resistance in the common carotid artery in the function of time.

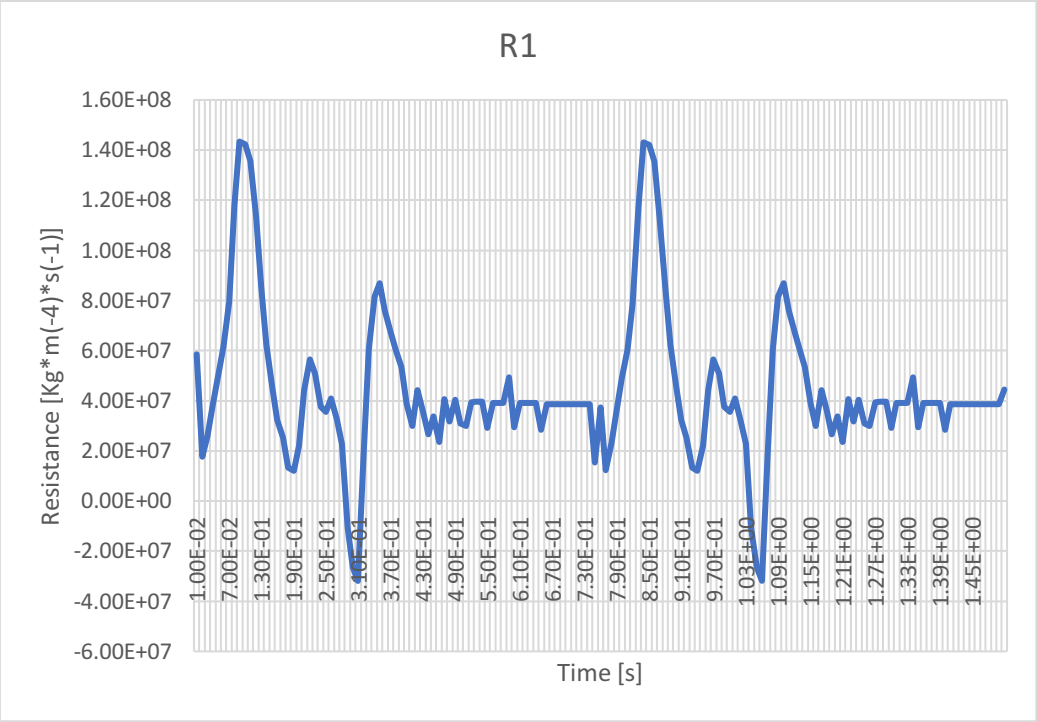

Figure 36. Resistance in the internal carotid artery in the function of time.

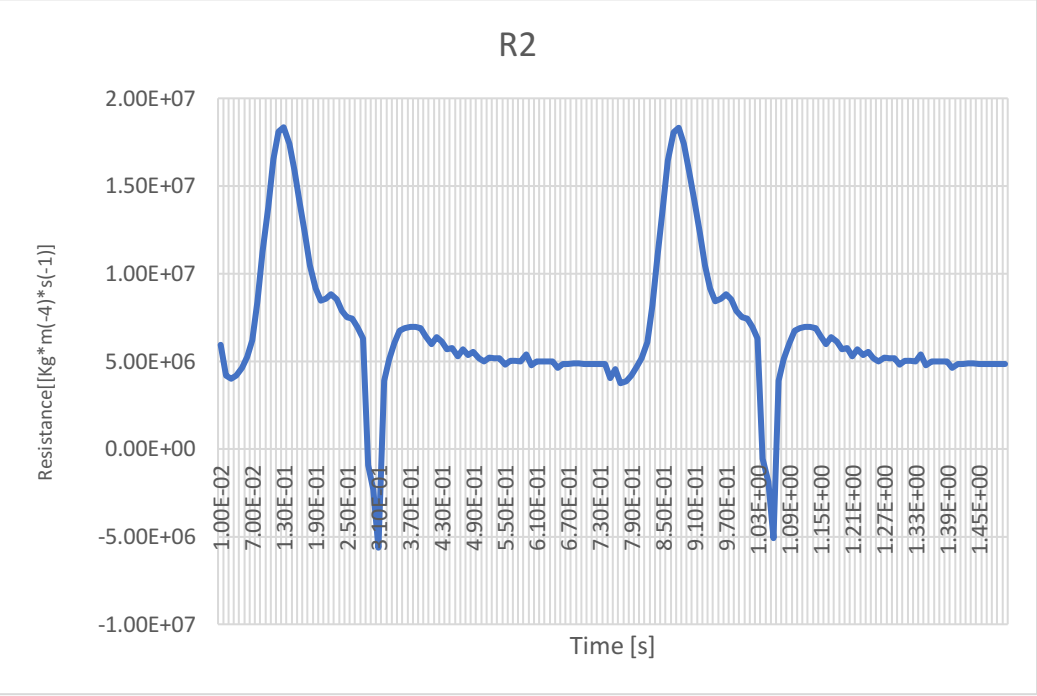

Figure 37. Resistance in the external carotid artery in the function of time.

3.2 3-mm plaques

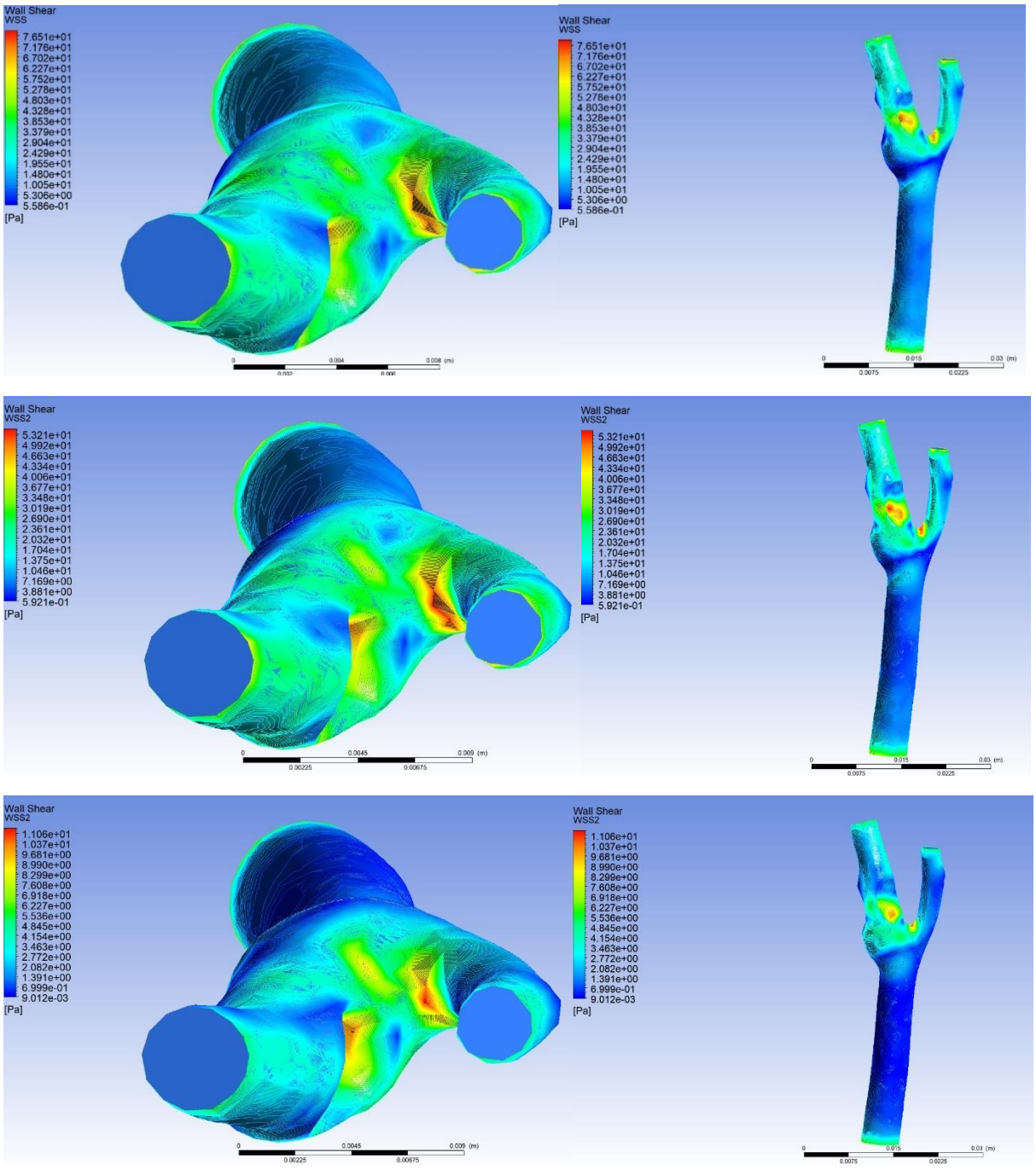

Figure 38. Representation of the WSS. Respectively in the first line the WSS at 0.13s, in the second line at 0.16s and in the third line at 0.31s.

As we can see from figure 38, although the bifurcation area presents high WSS values, in the period of maximum speed, the highest WSS values are found in the plaque opposite to the carotid sinus, with a maximum WSS value of 76 Pa. Although the values at the center of the plaque remain large compared to

those of the artery, as the velocity decreases, we observe instead that the maximum WSS tends to return to the bifurcation area.

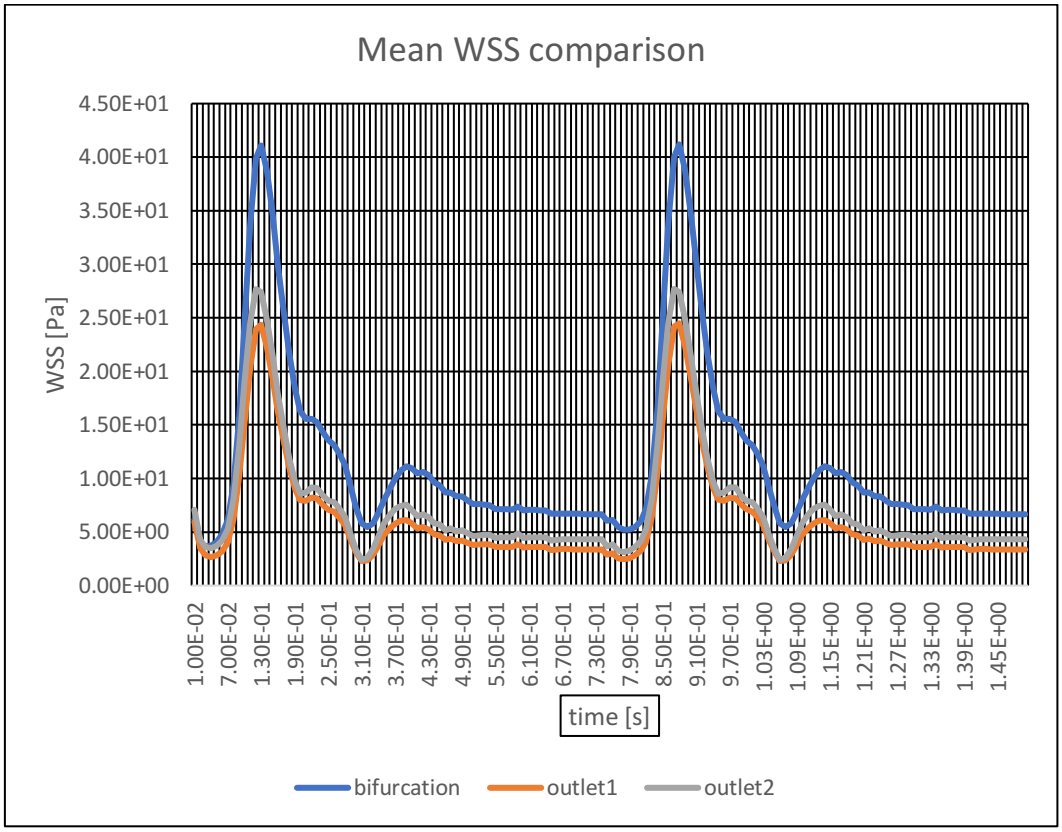

Figure 39. Mean WSS comparison between those of the wall_bifurcation (blue), wall_outlet1(orange) and wall_outlet2(grey).

Also in this case, we observe much higher WSS values in the bifurcation area than at the two outlets, as shown by figure 39. This time however, we observe higher WSS values at outlet 2 than at outlet 1 in the systolic phase, particularly at the time of maximum velocity at 0.13 s.

The following graphs highlight the percentage change in mean WSS of the case with occlusion, compared to the healthy case in the three different sections.

The mean WSS values were then obtained in the respective sections in the presence of plaques, from which the mean WSS values obtained for the healthy case were then subtracted. They were then normalized using the mean WSS in the healthy case and transformed into percentages.

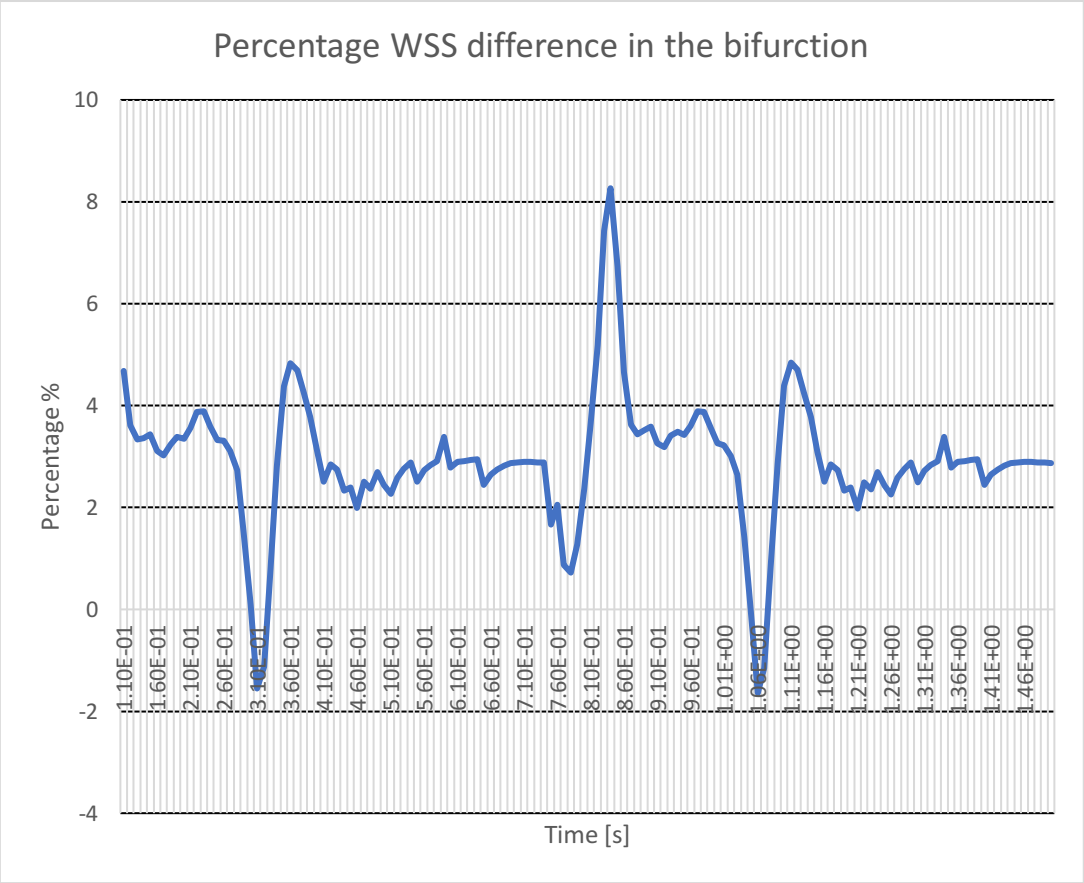

Figure 40. Graph showing the percentage change in WSS in the bifurcation between the case with 3-mm plaques and the healthy case.

Excluding the first values of the first cycle as errors in the simulation, we observe from figure 40, the mean WSS variation at the bifurcation. In particular, there seems to be the maximum variation in the WSS at 0.84s, which corresponds to the beginning of the phase of speed increase, variation of about 8%. We also observe a decrease, albeit negligible (1%) in the times of lower speed value (respectively 0.31s and 1.06s). In the constant velocity systolic phase, the variation remains constant and always positive. Therefore generally, we can conclude that in the bifurcation area there is an increase in mean WSS in the case of this occlusion.

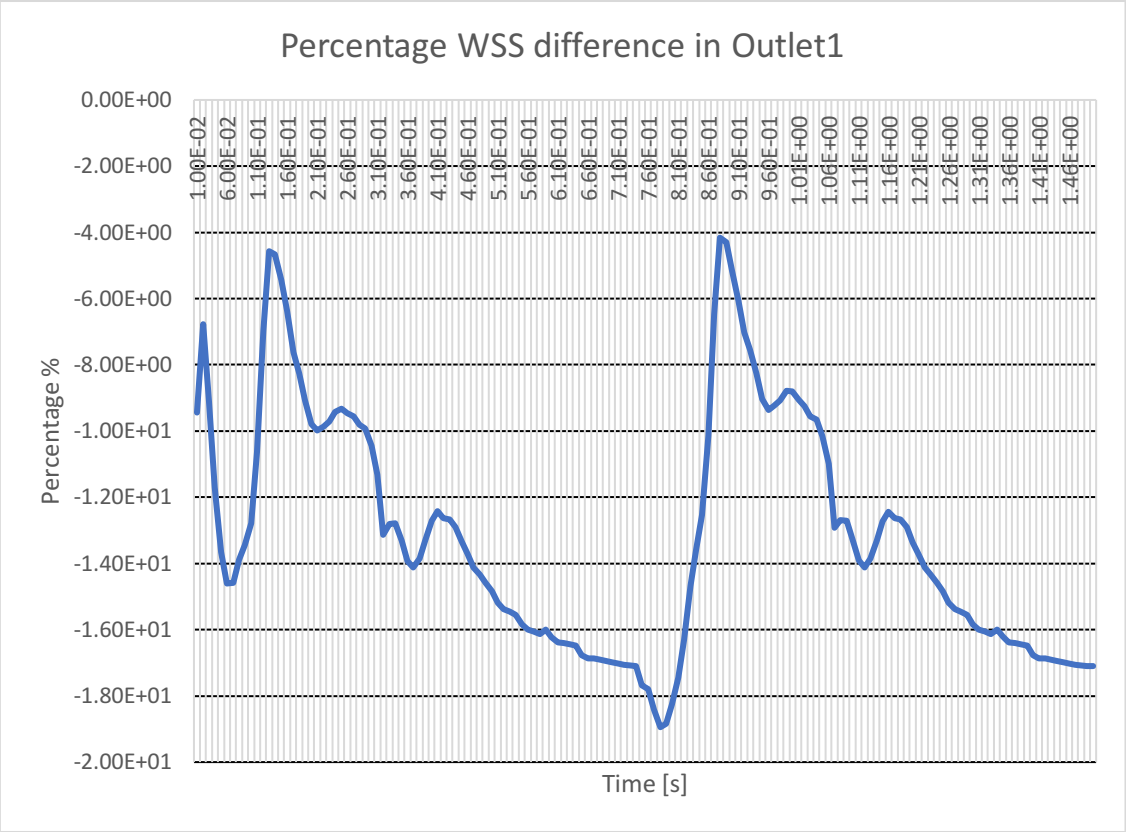

Figure 41. Graph showing the percentage change in WSS in wall_outlet 1 between the case with 3-mm plaques and the healthy case.

In wall_outlet 1, where the occlusion is therefore present, we observe a general decrease in the WSS. In this case, the least variation is precisely in correspondence with the systolic phase when the speed is maximum (0.13 s), which is around 4 %. During the systolic phase at a more or less constant speed, we instead observe a decrease in the WSS in case of obstruction. In fact, the maximum variation, around 19%, is found between the beginning of the systolic phase and the end of the diastolic phase (0.79s).

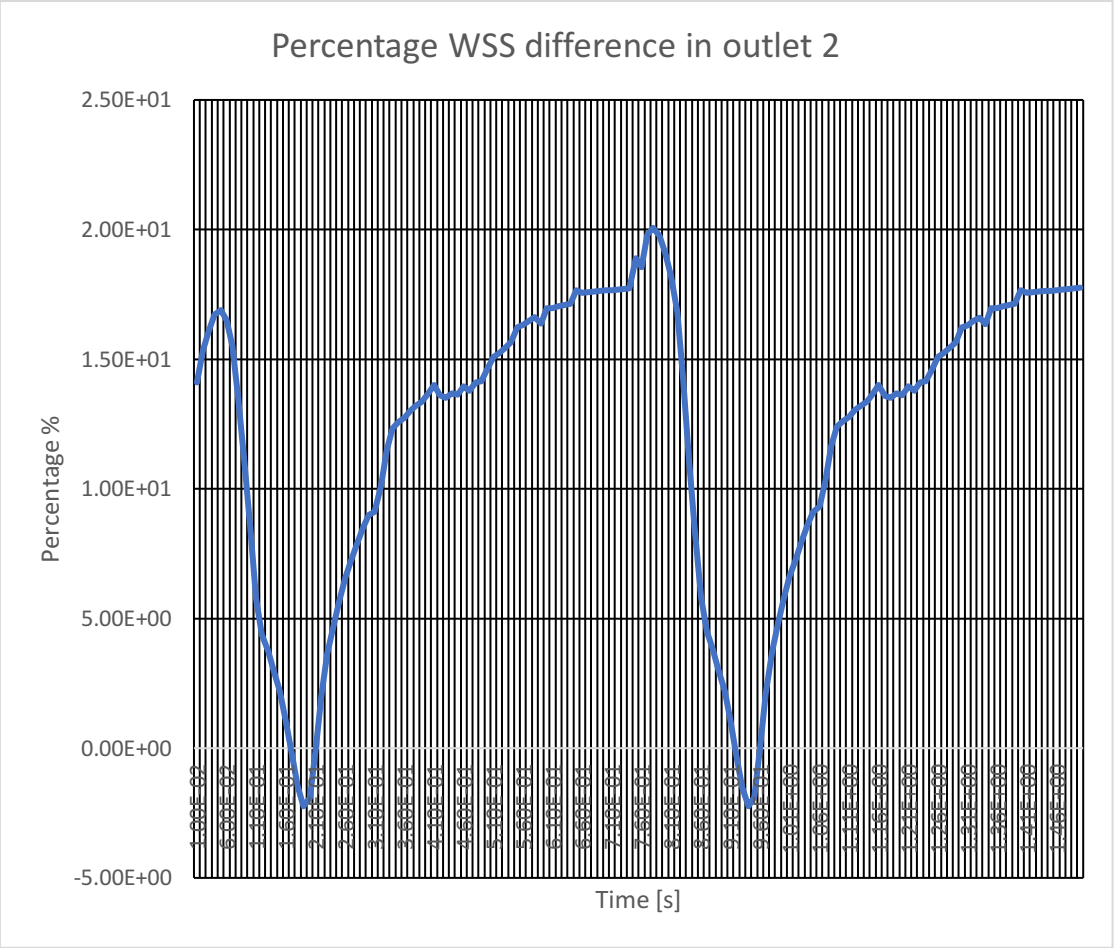

Figure 42. Graph showing the percentage change in WSS in wall_outlet 2 between the case with maximum occlusion and the healthy case

In wall_outlet 2 instead, we register a general increase in the WSS. Here instead of a decrease in the constant velocity systolic phase, we find an increase. The times of smaller variation, which correspond to a decrease in the WSS, are recorded respectively at 0.19s and 0.95s, which correspond to two points in the speed decrease phase. The maximum variation time, on the other hand, correspond to the same as for wall_outlet 1, therefore corresponding to the beginning of the speed increase phase (0.79s) in which we have an increase of WSS of about 20%.

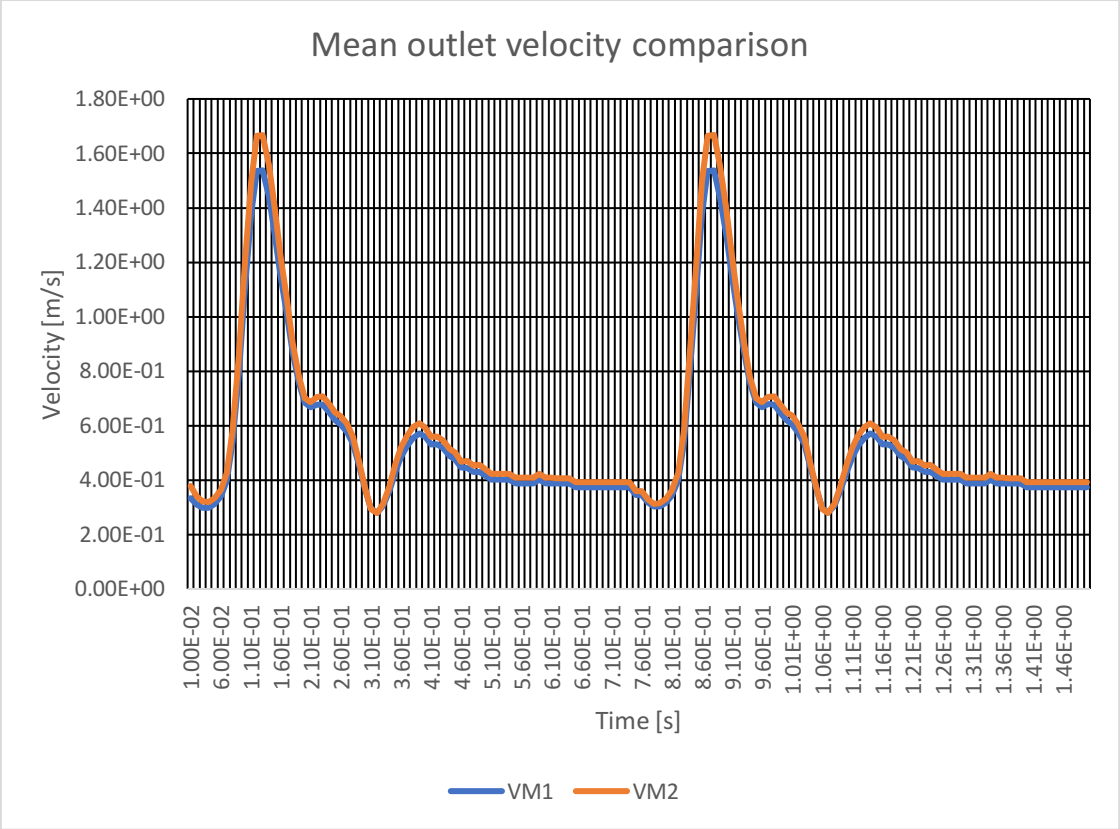

Figure 43. Comparison of the average speeds between outlet 1 (blue) and outlet 2 (orange).

With reference to figure 43, we observe, that in this case, unlike the healthy one (figure 33), higher average speed values are present at outlet 2 than at outlet 1, especially at the time of maximum speed at 0.13s. The difference becomes negligible at the time of minimum speed at 0.31s.

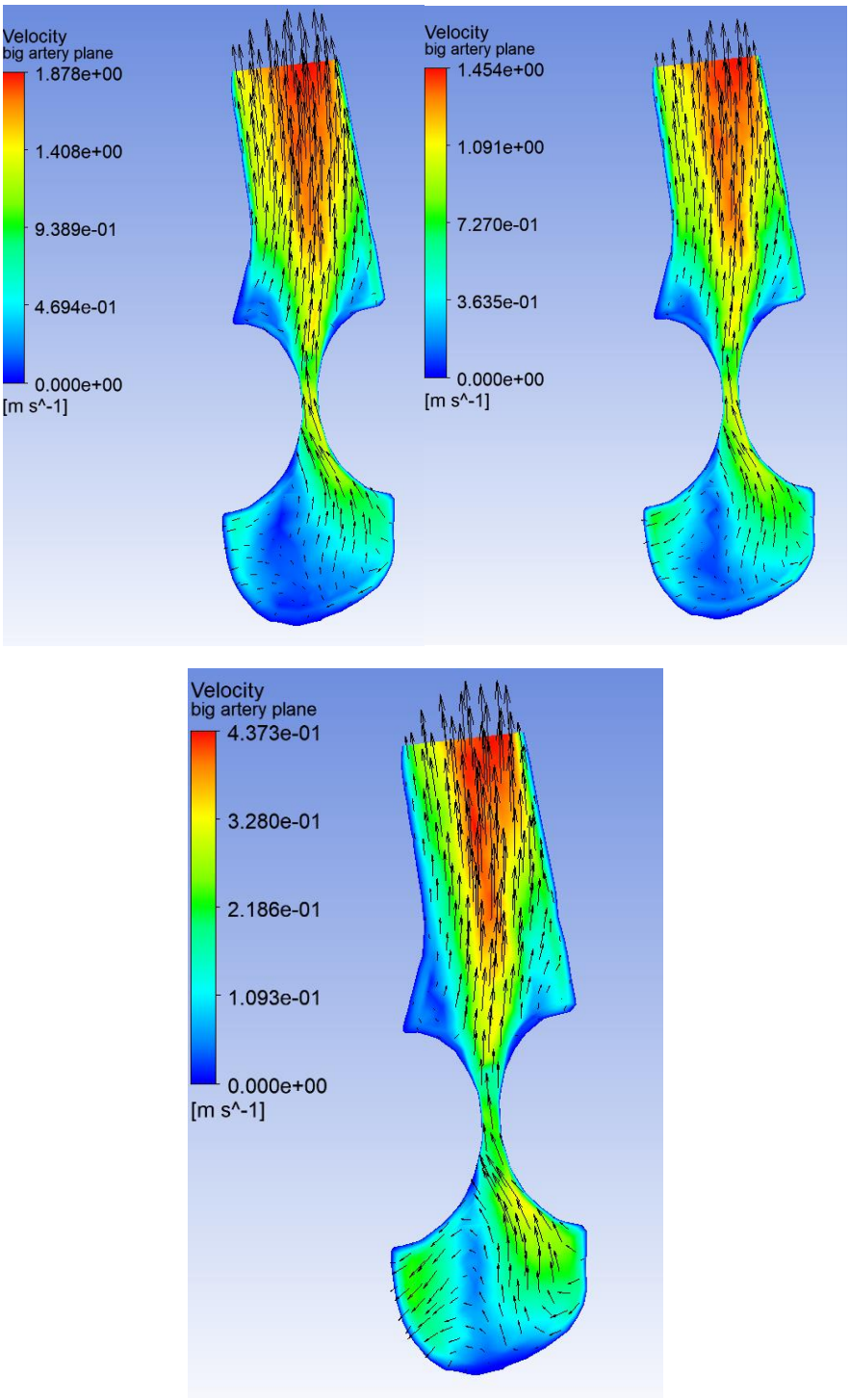

Figure 44. Color map and vector plot of the local velocity. On the top left,0.13s, top right, 0.16 and bottom instead 0.31s.

Figure 44 shows how the velocity profile does not vary appreciably between instants 0.13s and 0.16s. The maximum speed is always observed shortly after the occlusion, which suggests that it is the bottleneck itself that increases its speed. Variations of the velocity profile also occur upstream of the occlusion as can be seen

from figure 44, in particular at time of 0.31s. In fact, the obstruction generates local flows in the carotid sinus which then impact against the vessel wall.

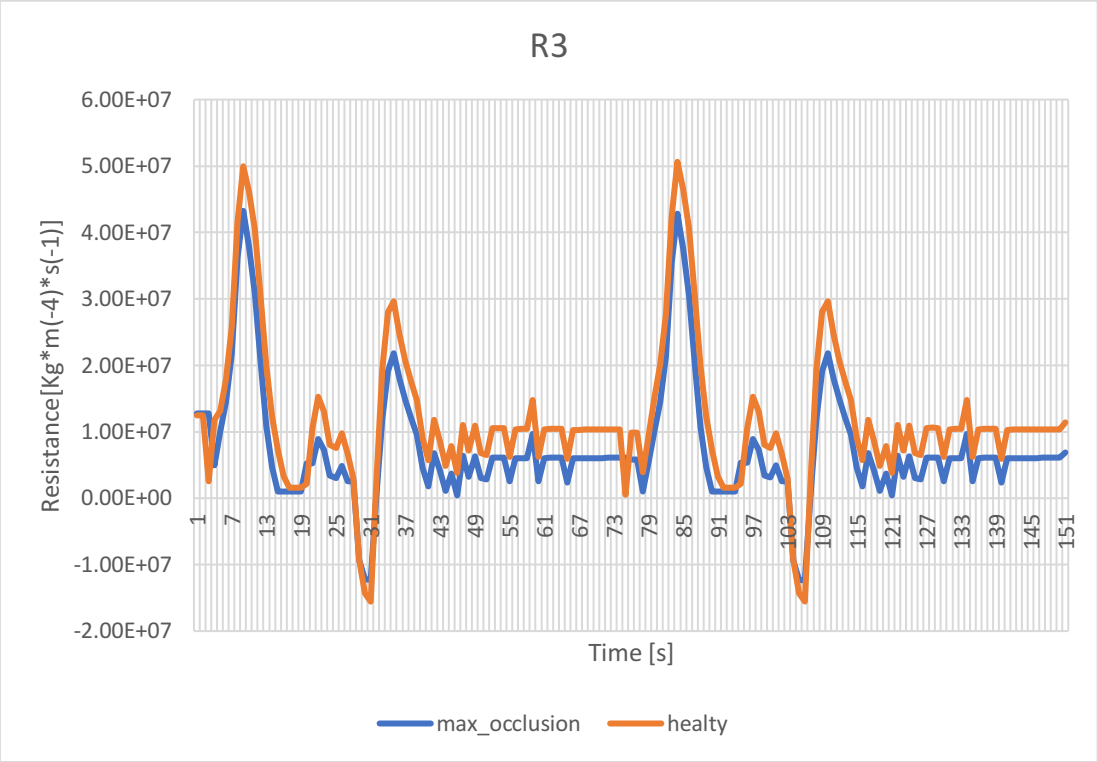

Figure 45. Comparison of resistance values between artery with 3-mm plaques (blue) and healthy artery (orange) in the common carotid artery.

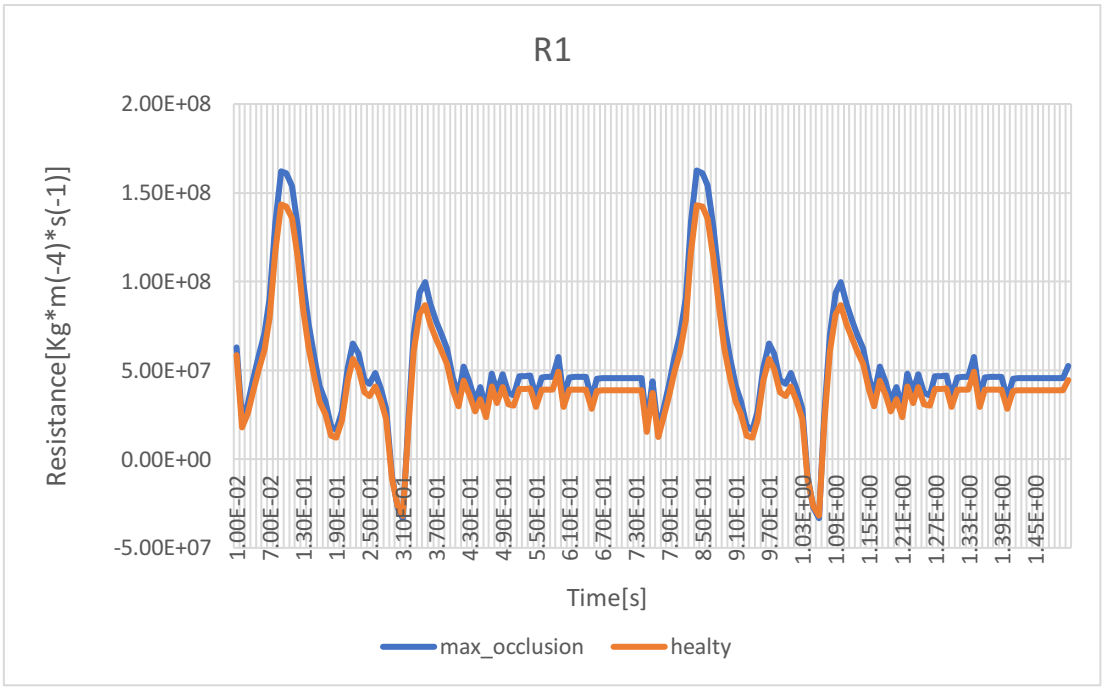

Figure 46. Comparison of resistance values between artery with 3-mm plaques(blue) and healthy artery (orange) in the internal carotid artery.

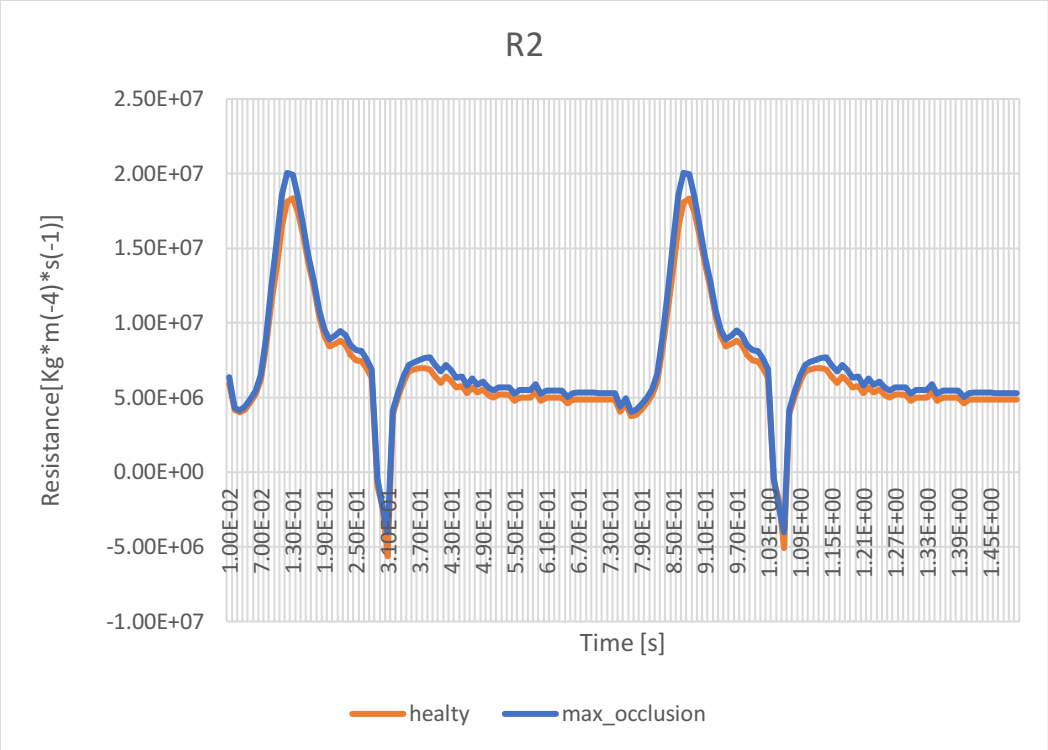

Figure 47. Comparison of resistance values between artery with 3-mm plaques (blue) and healthy artery (orange) in the external carotid artery.

From the above figures(figures 45-45-47) we observe that the artery with the occlusion, generally presents higher resistance values in the artery where the occlusion is present (R1), i.e. the internal carotid artery and also in the external carotid artery (R2). In the common carotid artery instead (R3), we observe a general decrease.

3.3 2-mm plaques

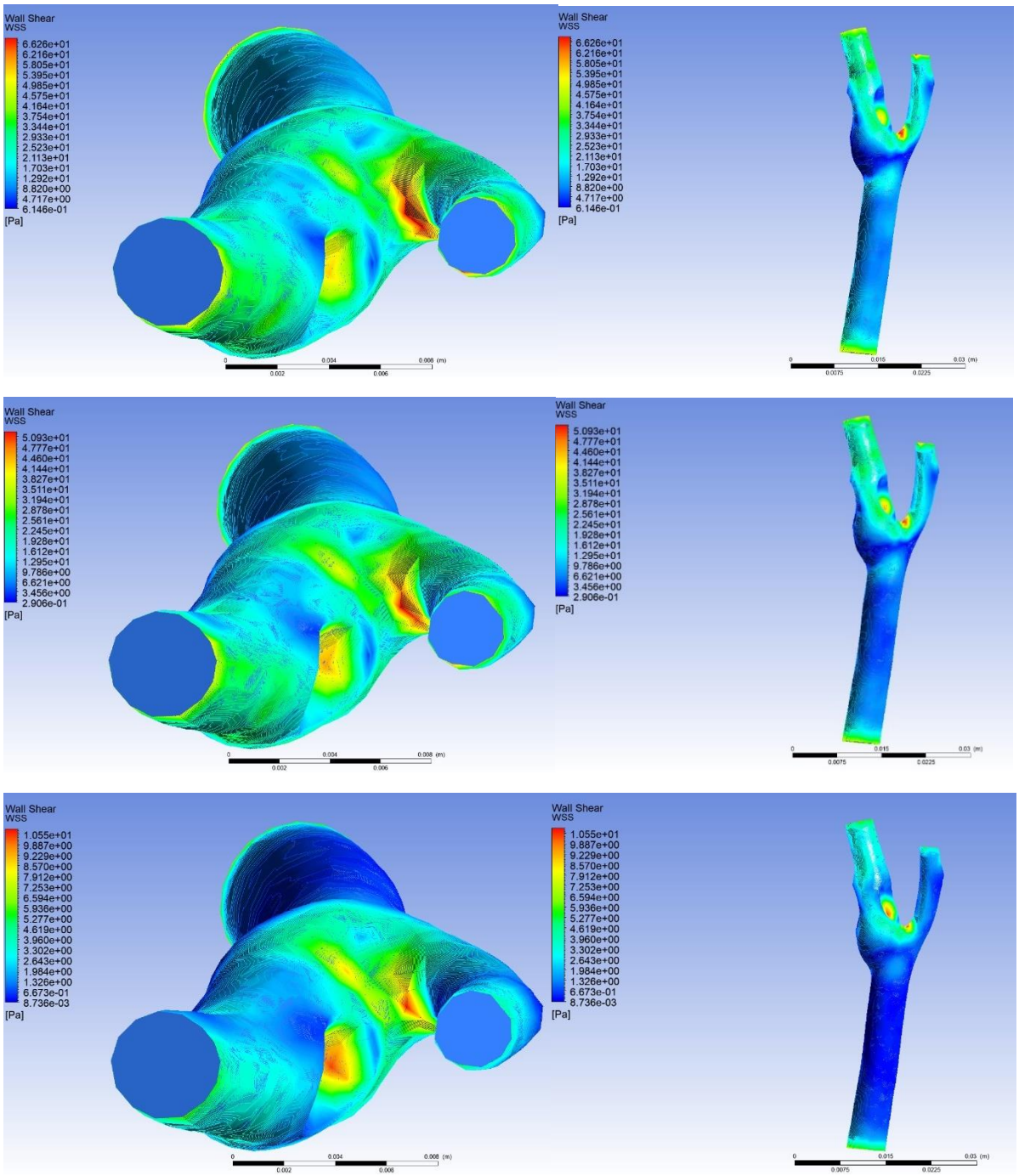

Figure 48. Representation of the WSS. Respectively in the first line the WSS at 0.13s, in the second line at 0.16s and in the third line at 0.31s

Observing figure 48, we note that for instants 0.13s and 0.16s the maximum values of WSS are located in the usual zone of the bifurcation, although the plaque area still has high values. However, as the speed decreases, the maximum WSS values tend to concentrate also on the plaque.

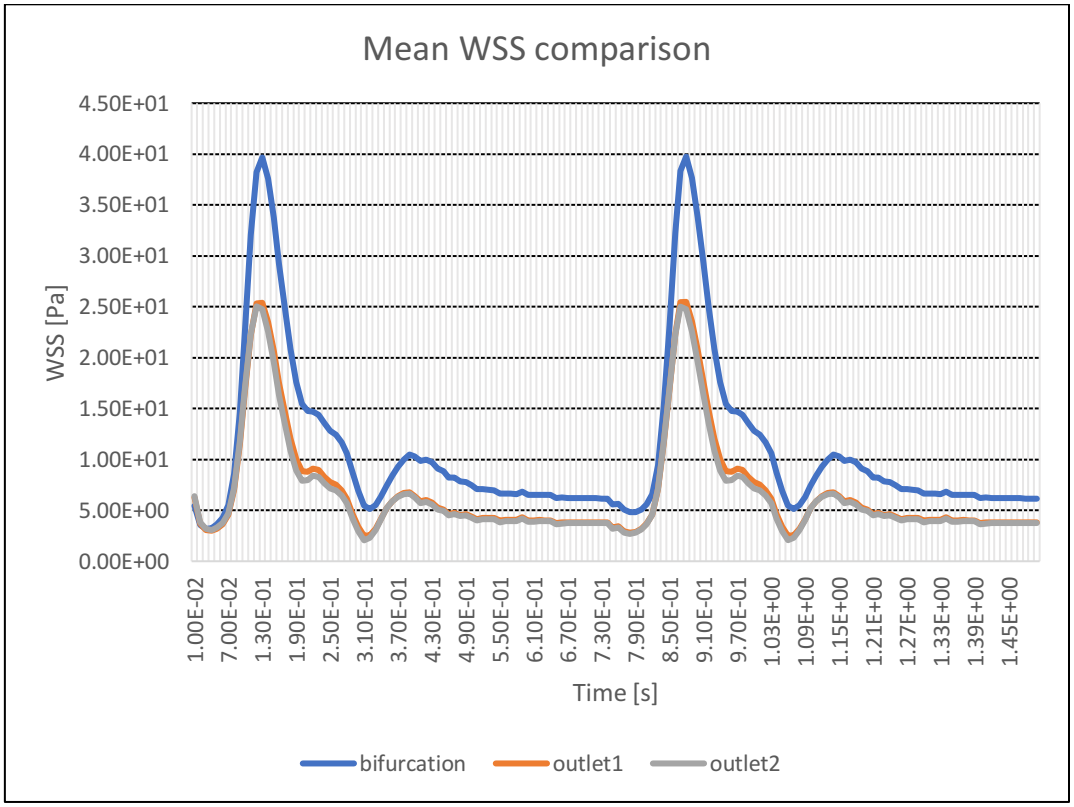

Figure 49. Mean WSS comparison between those of the wall_bifurcation (blue), wall_outlet1 (orange) and wall_outlet2 (grey).

With reference to figure 49, also in this case, the mean WSS values at the bifurcation are much higher than those of the 2 outlets. Although the mean WSS values at the two outlets show greater differences compared to the healthy case, they show smaller differences when compared to the case with the maximum occlusion.

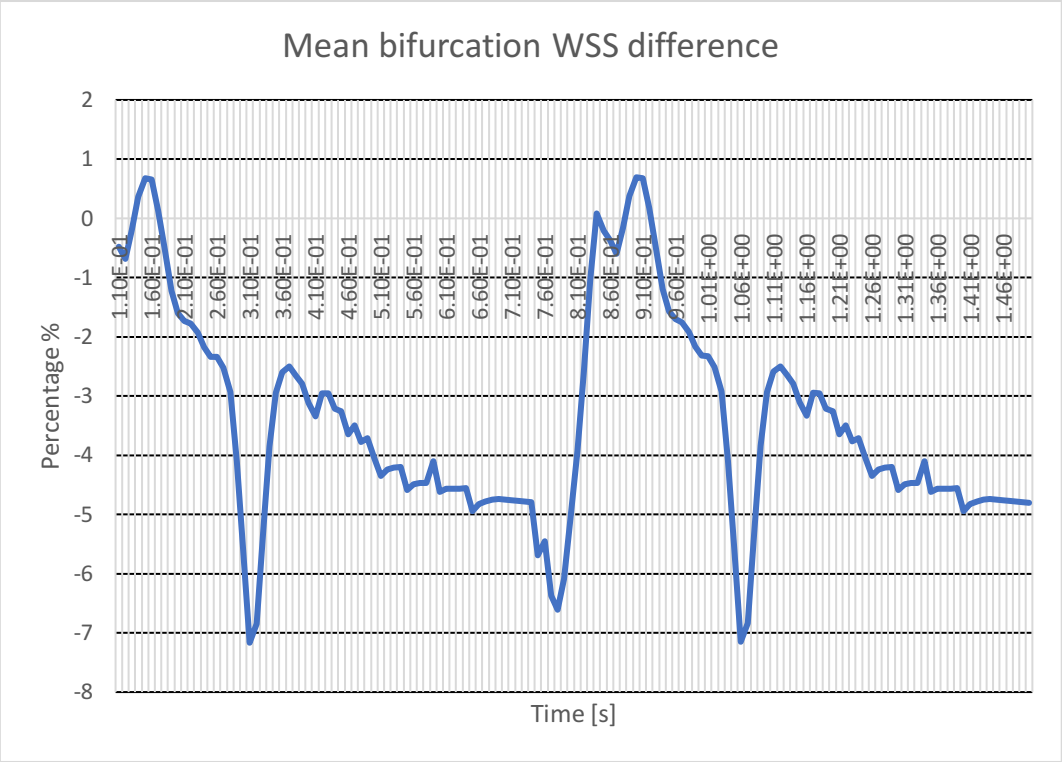

Figure 50. Graph showing the percentage change in WSS in the wall_bifurcation between the case with occlusion and the healthy case.

Figure 50, also here referring only to the second cycle, shows how, unlike the case with the maximum obstruction, in this case a general decrease in the mean WSS occurs, the maximum variation is in the time of minimum speed(-7%). An insignificant increase is found between 0.83s and 0.97s, when the speed is in the ascending phase.

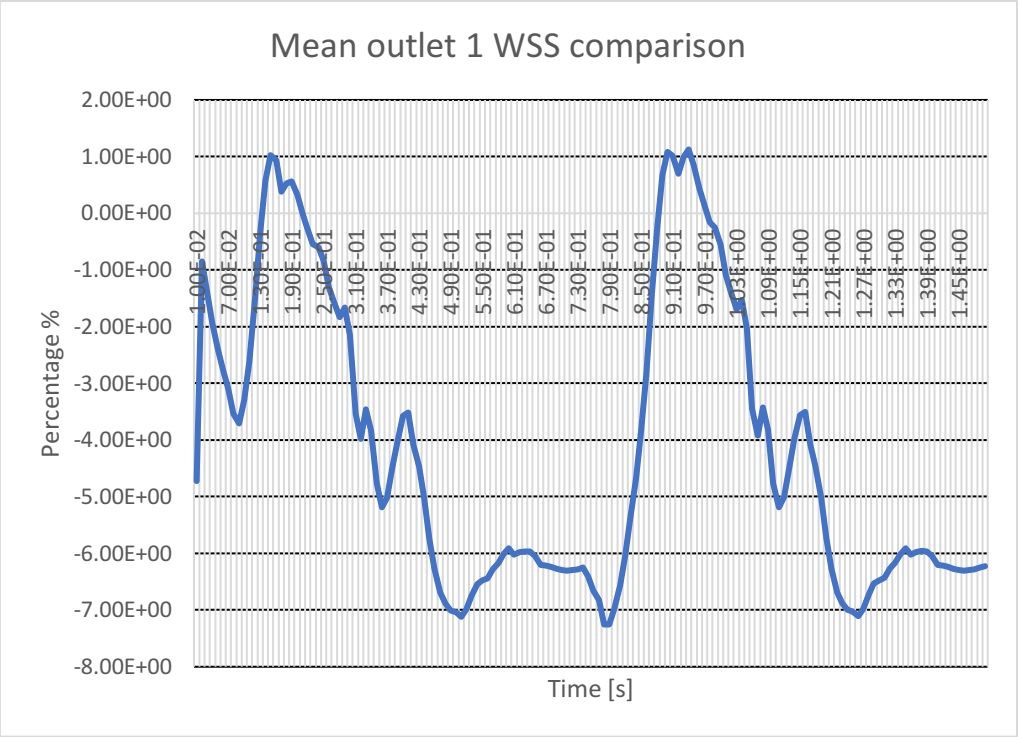

Figure 51. Graph showing the percentage change in WSS in wall_outlet 1 between the case with occlusion and the healthy case

Figure 51, shows a general decrease, albeit smaller than in the case with maximum occlusion, of the WSS values at wall_outlet 1. The greatest variation, between 0.5s and 0.78 s, is found in correspondence with the almost constant speed of the diastolic phase (-7%), and a slight positive variation in the section where the speed decreases (1%).

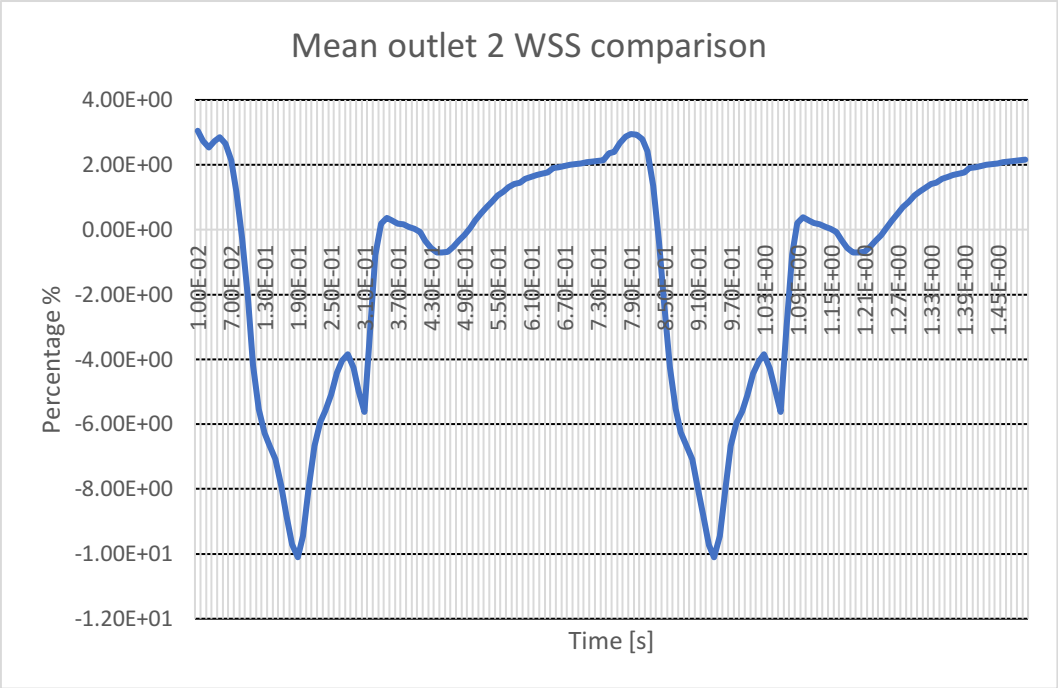

Figure 52. Graph showing the percentage change in WSS in wall_outlet 2 between the case with occlusion and the healthy case.

Looking at figure 52, we observe a general decrease also at wall_outlet2, with a maximum variation of 10%. A slight increase instead occurs between 0.34s and 0.85s, which includes the systolic phase and part of the speed increase phase (3%)

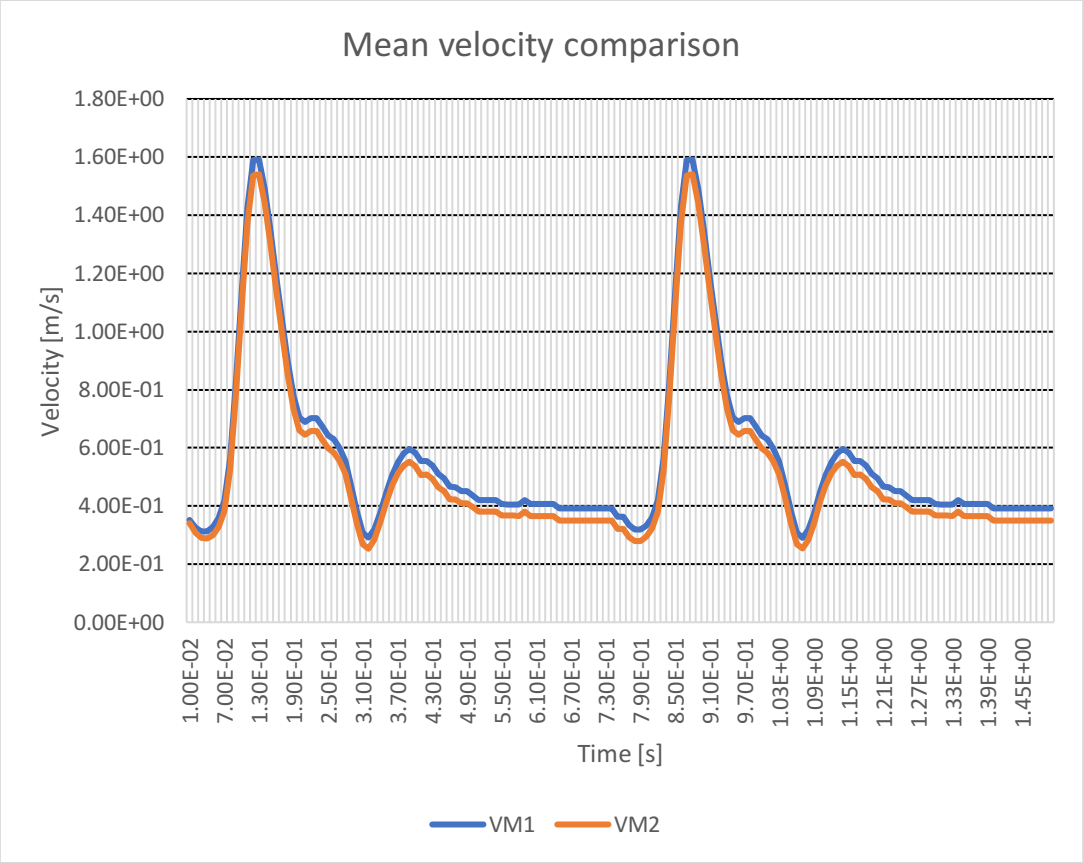

Figure 53. Comparison of the average speeds between that of outlet 1(blue) and that of outlet 2(orange).

Figure 53 illustrates how the velocity outgoing from outlet1 (internal carotid artery) is larger than that outgoing from outlet2 (internal carotid artery)

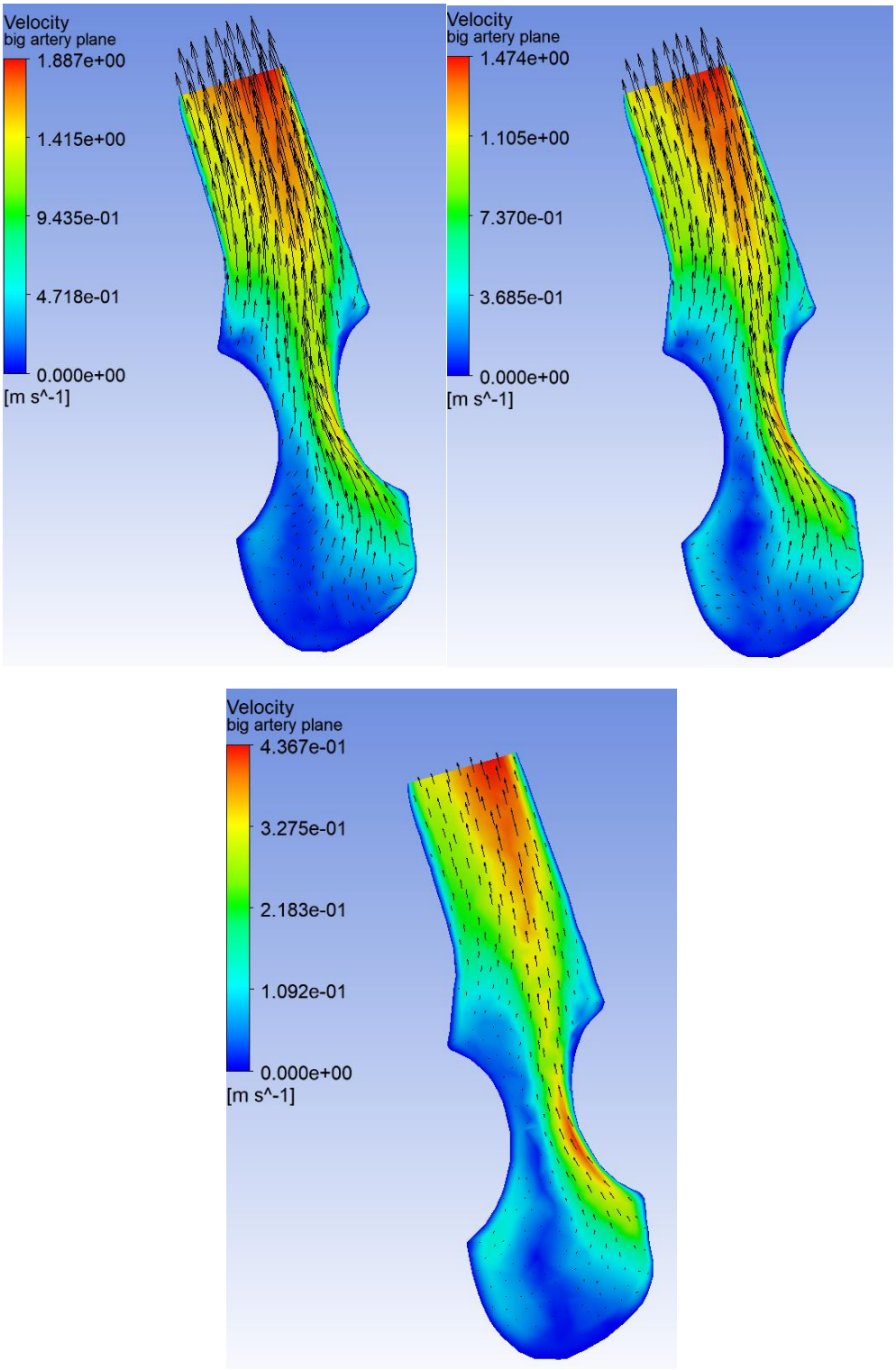

Figure 54 . Color map and vector plot of the local velocity. On the top left,0.13s, top right,0.16 and bottom instead 0.31s

The upper figure 54 reveals, again, how the maximum speed tends to be at the end of outlet1. However, as the speed decreases, we note that high speed values tend to be in correspondence with the plaque. Also in

this case, the left plaque seems to generate a speed recirculation upstream of it, even if of less entity than in the case of maximum obstruction.

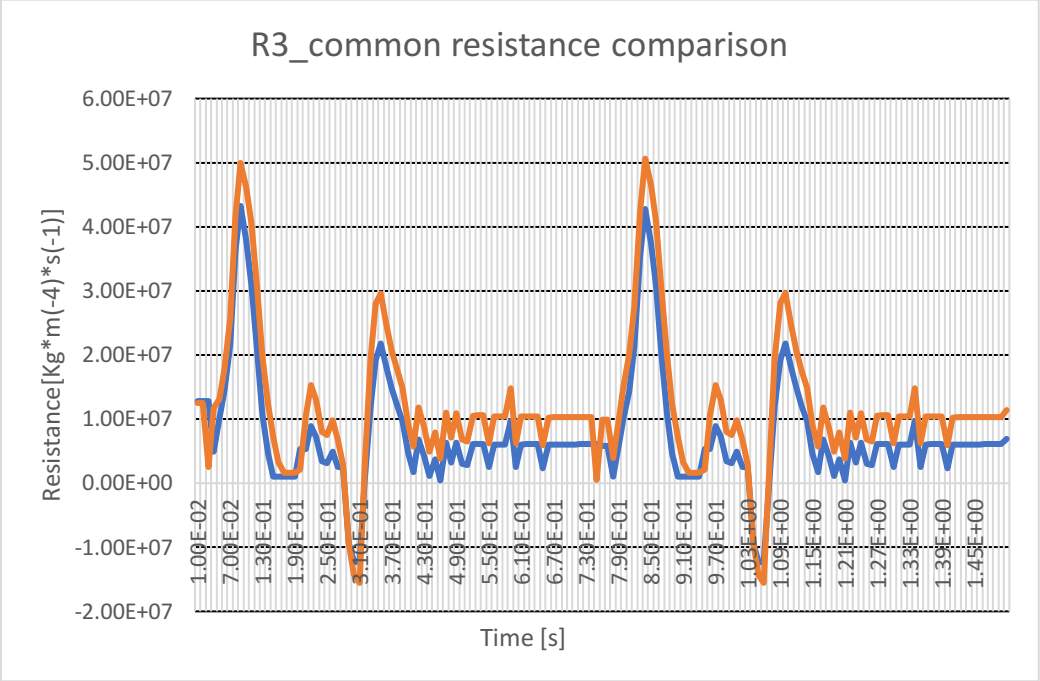

Figure 55. Comparison of resistance values between artery with 2-mm plaques (blue) and healthy artery (orange) in the common carotid artery.

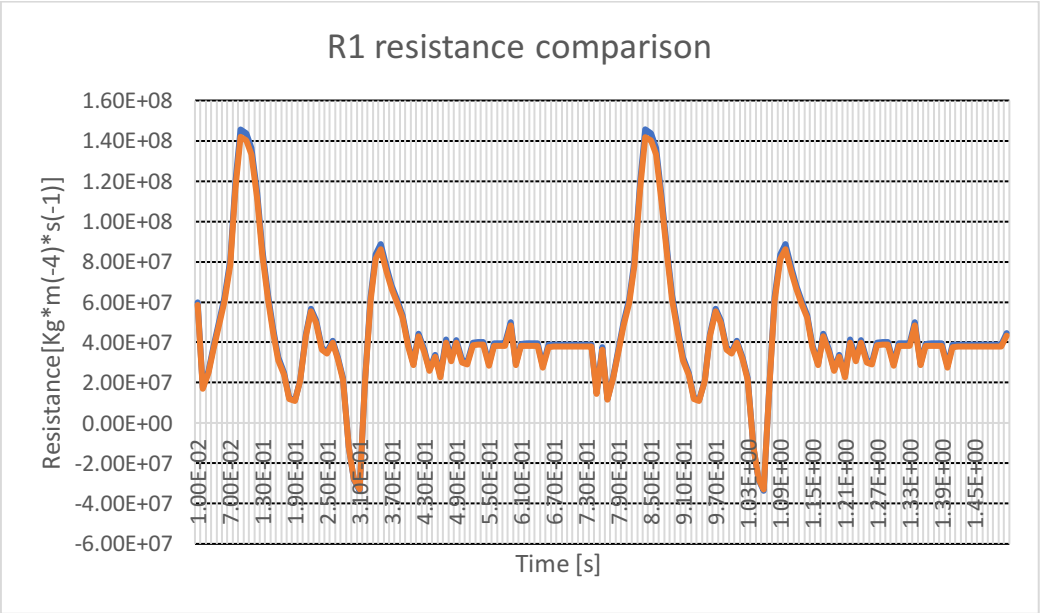

Figure 56. Comparison of resistance values between artery with 2-mm plaques (blue) and healthy artery (orange) in the internal artery.

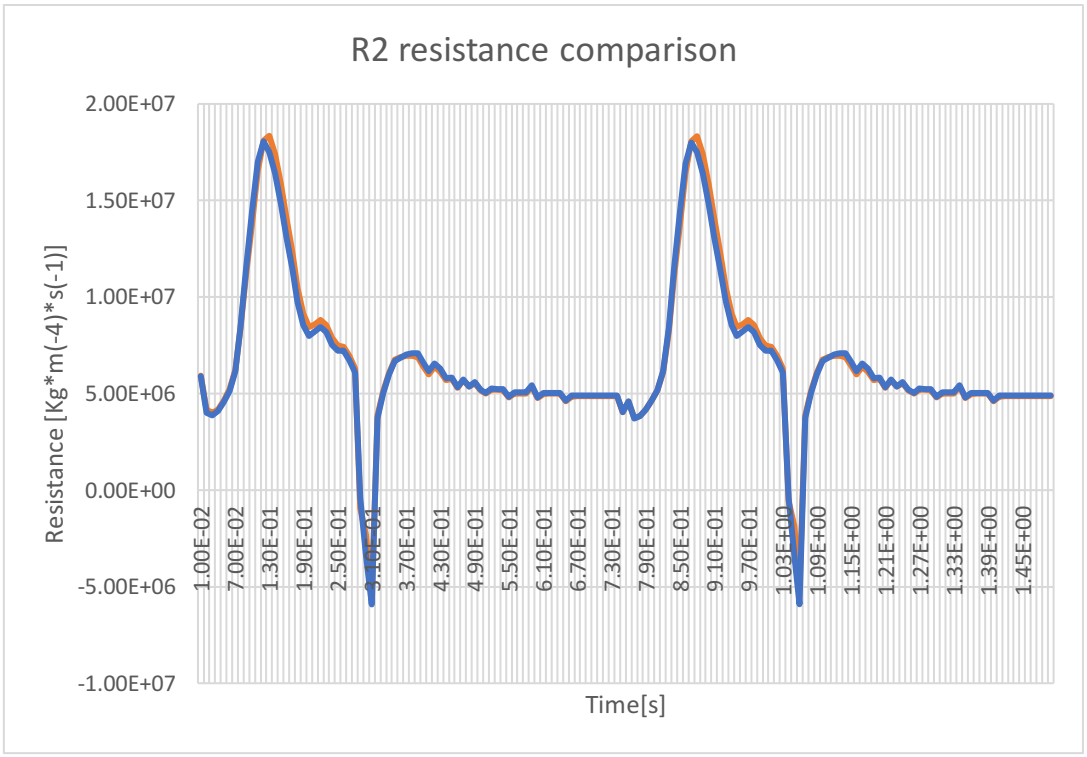

Figure 57. Comparison of resistance values between artery with 2-mm plaques (blue) and healthy artery (orange) in the external artery.

Figures 55-56-57 show that greatest resistance variation seems to be in the common carotid artery, where the healthy case shows higher resistance values. In the internal artery, on the other hand, a slight increase in resistance is observed in the case with occlusion. Slightly higher values of resistance are also found in the internal artery in the healthy case.

3.4 1-mm plaque

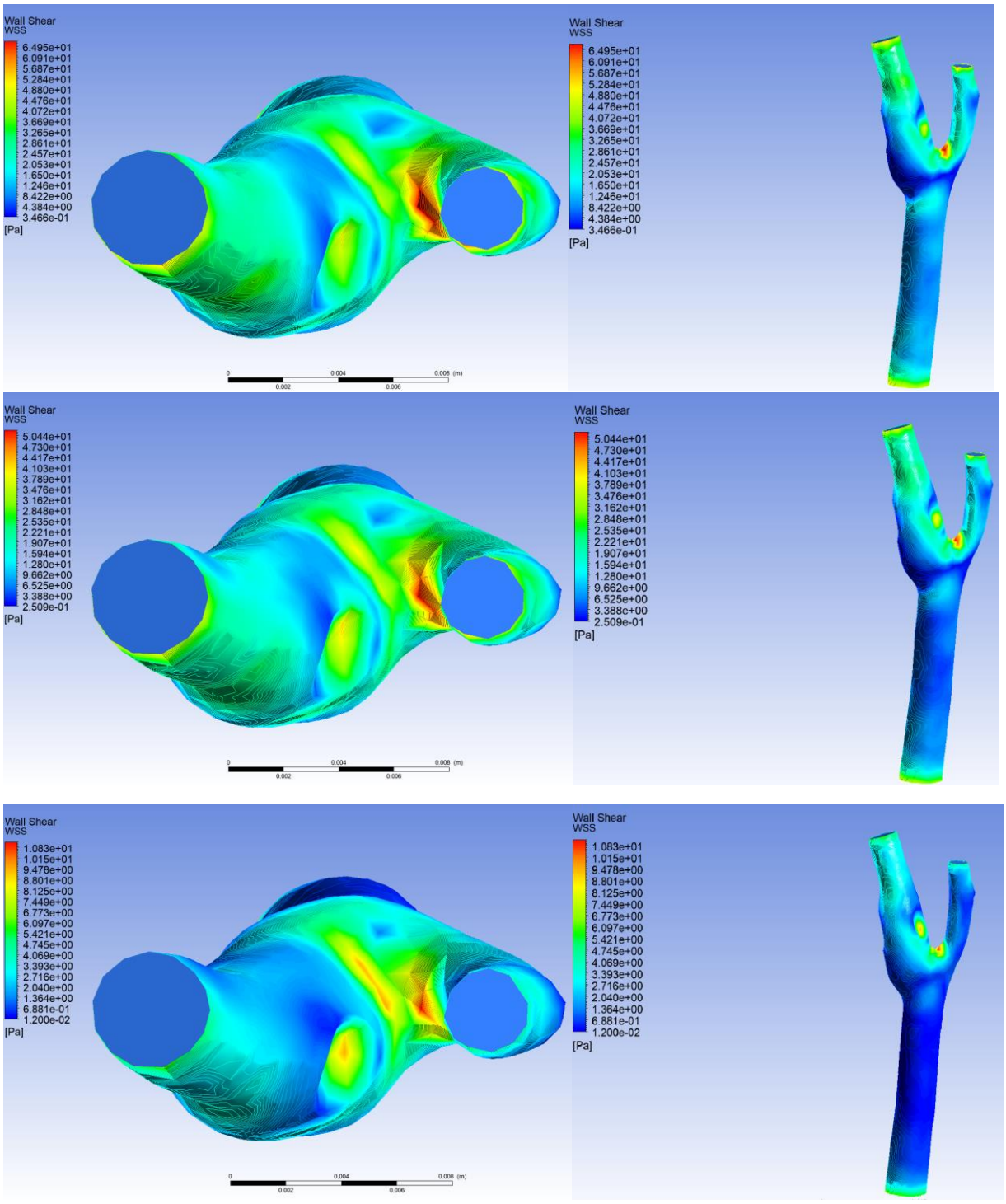

Figure 60. Representation of the WSS. Respectively in the first line the WSS at 0.13s, in the second line at 0.16s and in the third line at 0.31s.

Looking at figure 60 we conclude that the distribution of WSS is similar to that of the previous case, since at times 0.13s and 0.16s, the maximum values of WSS are in correspondence with the bifurcation adjacent to the internal carotid artery. Although even here the values in the plaque area are still high, especially at 0.31s, the maximum values tend to remain in the bifurcation area. We also observe how at 0.31s higher WSS values are also found in the area of the bifurcation closest to the internal artery, similar to what happened in the healthy case. In this case, the maximum WSS value is 64.9 Pa

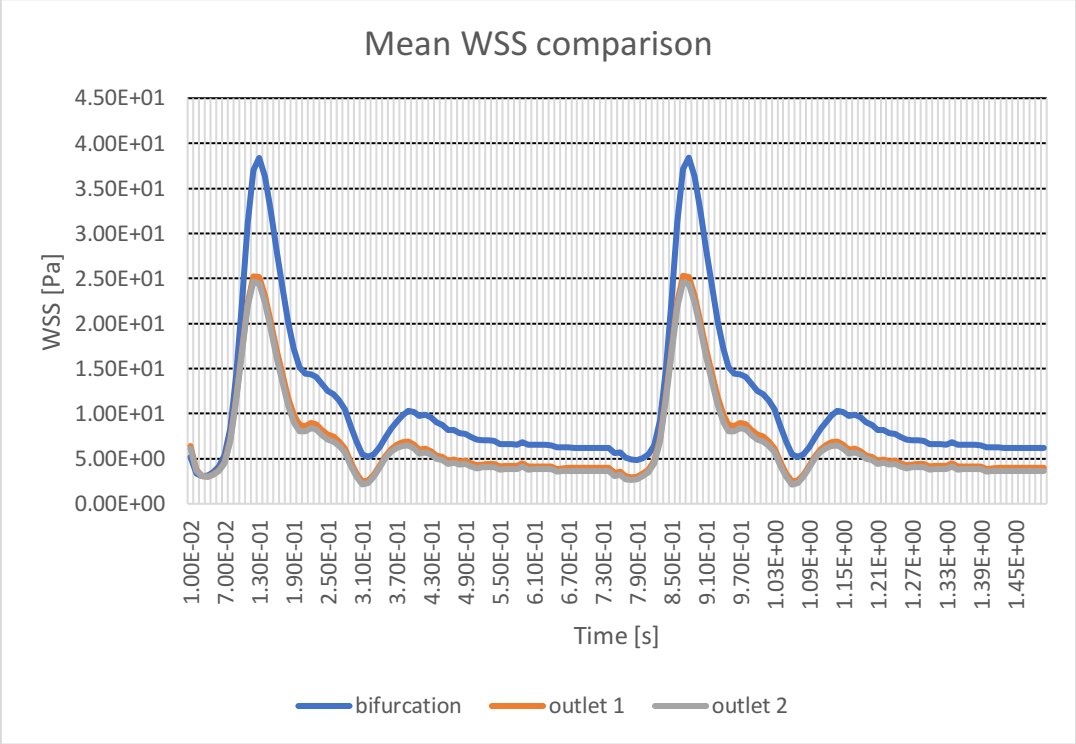

Figure 61. Mean WSS comparison between those of the wall_bifurcation (blue), wall_outlet1 (orange) and wall_outlet2 (grey).

Figure 61 reveals how, like all previous cases, the mean WSS values of the bifurcation are greater than those of the two outlets.

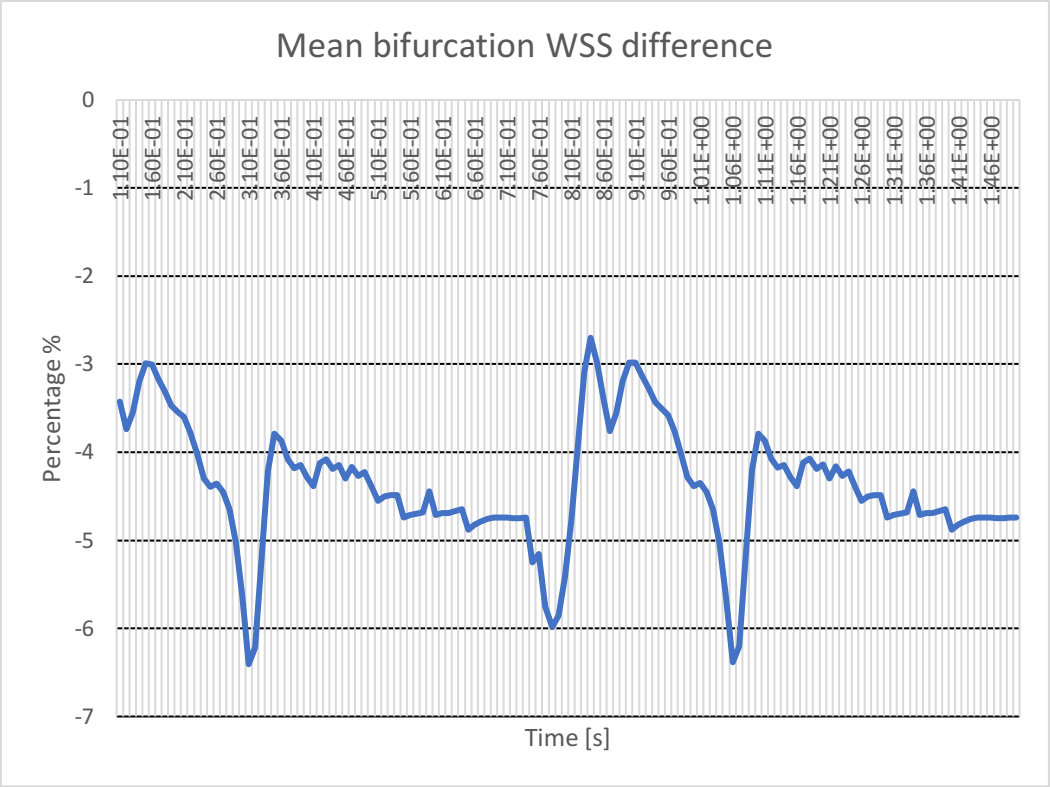

Figure 62. Graph showing the percentage change in WSS in the bifurcation between the case with occlusion and the healthy case.

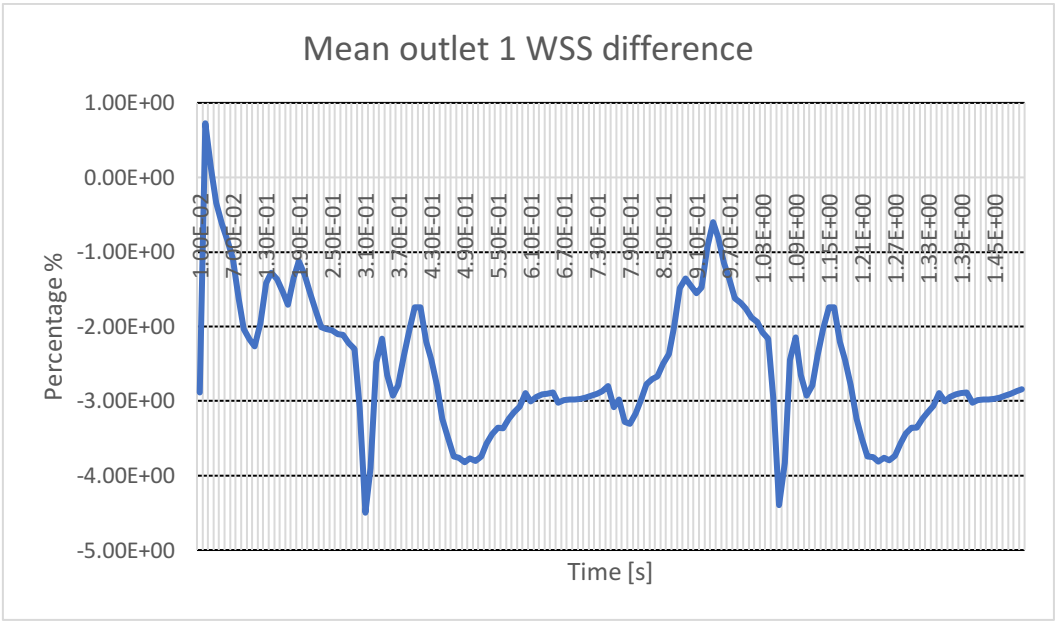

Figure 63. Graph showing the percentage change in WSS in the wall_outlet1 between the case with occlusion and the healthy case.

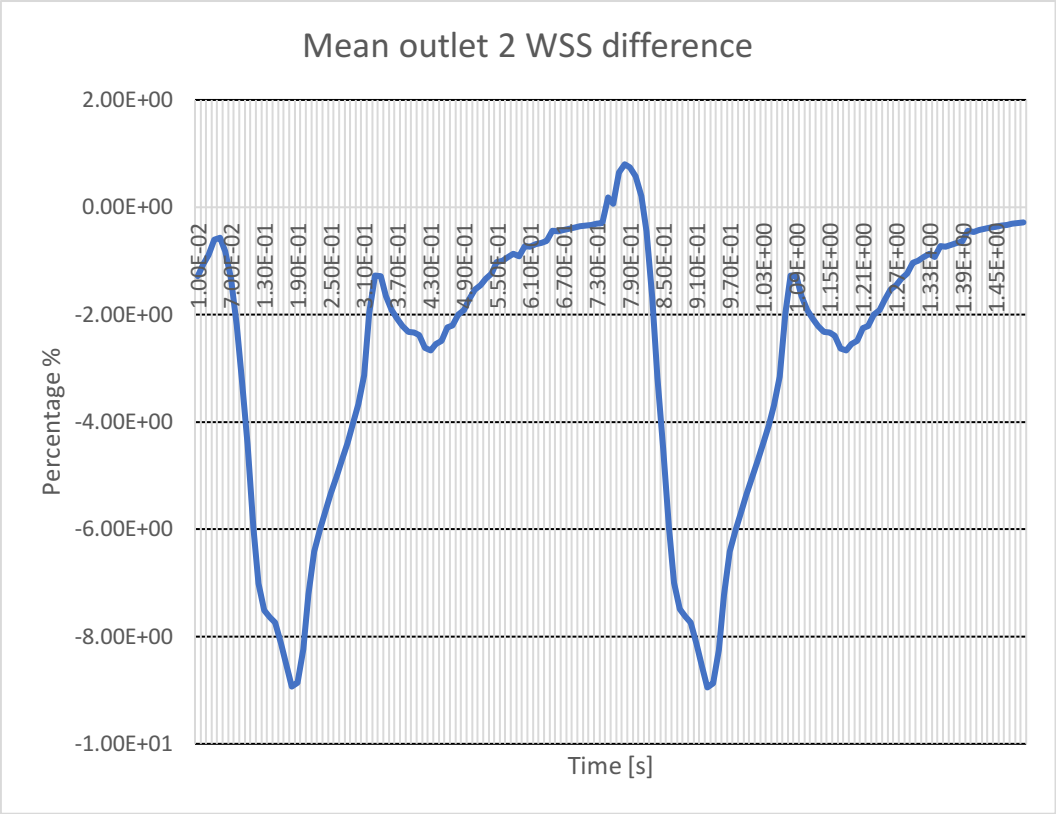

Figure 64. Graph showing the percentage change in WSS in wall_outlet 2 between the case with occlusion and the healthy case.

From the figures 62-63-64 we observe that trends in the percentage variations of the mean WSS are similar to those recorded for the case of 2-mm plaques, although these present lower variations values.

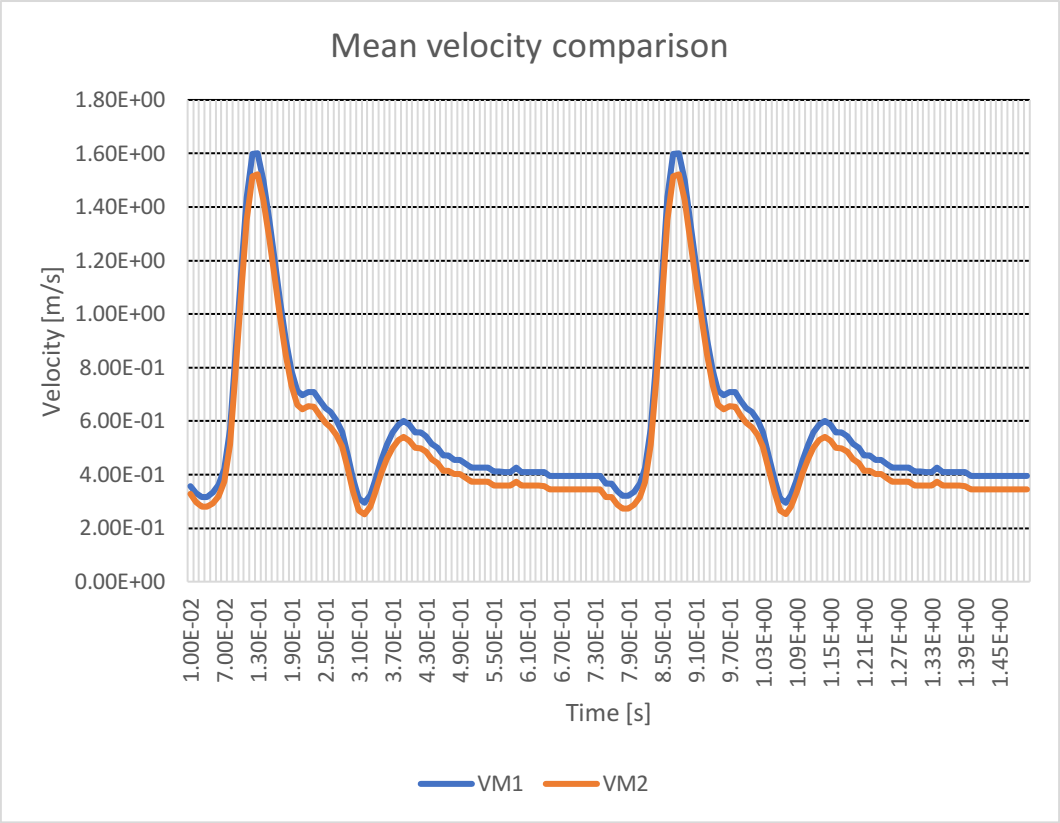

Figure 65. Comparison of the average speeds between outlet 1(blue) and outlet 2(orange).

Observing figure 65, we note that also in this case the average speed leaving outlet1 is greater than that leaving outlet2.

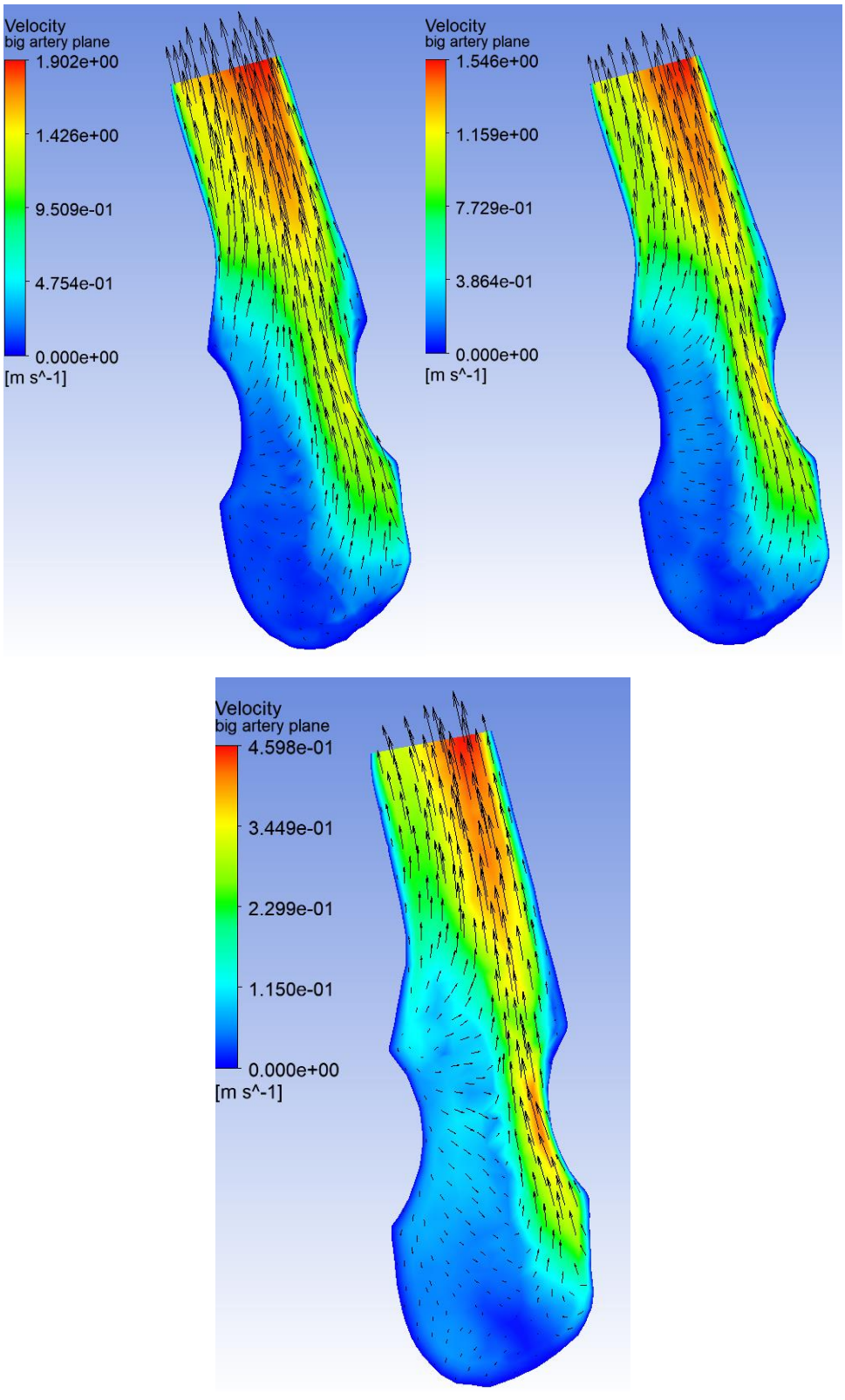

Figure 66. Color map and vector plot of the local velocity. On the top left,0.13s, top right,0.16 and bottom instead 0.31s

With reference to figure 66, we observe how the velocity behavior is more similar to the healthy case, although the recirculation velocity of the carotid sinus still seems to have less influence in the minimum

velocity phase due to the presence of the plaques. However, downstream of these, lower velocity values are observed compared to the cases with larger plaques.

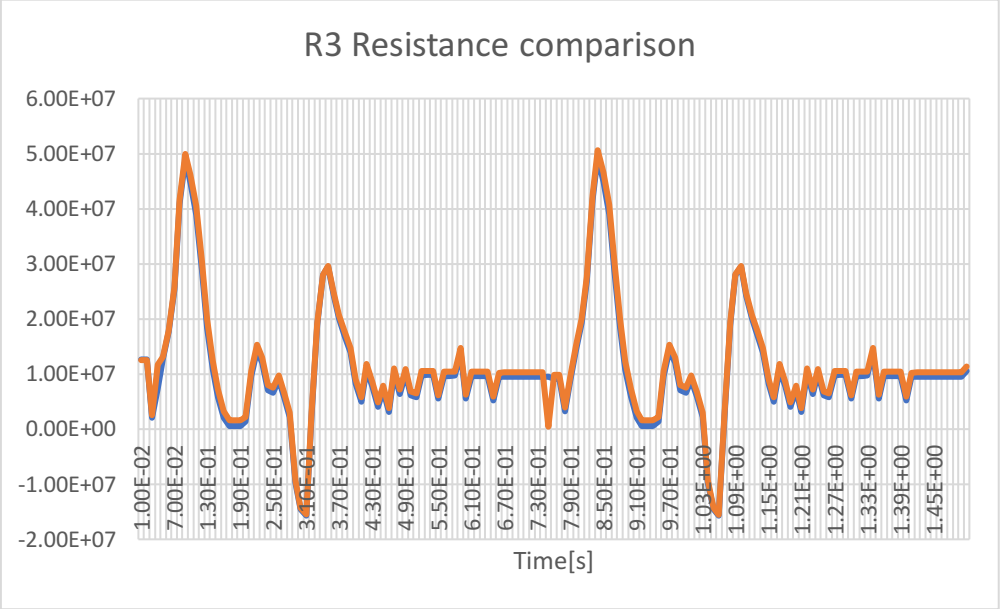

Figure 55. Comparison of resistance values between artery with 1-mm plaques (blue) and healthy artery (orange) in the common carotid artery.

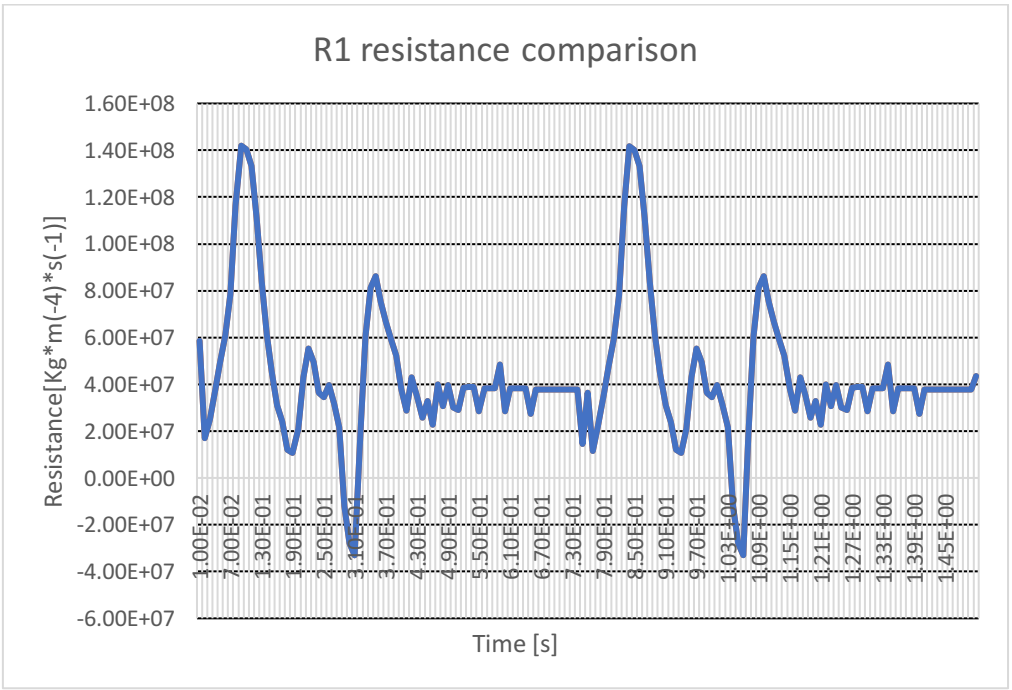

Figure 56. Comparison of resistance values between artery with 1-mm plaques (blue) and healthy artery (orange) in the internal carotid artery.

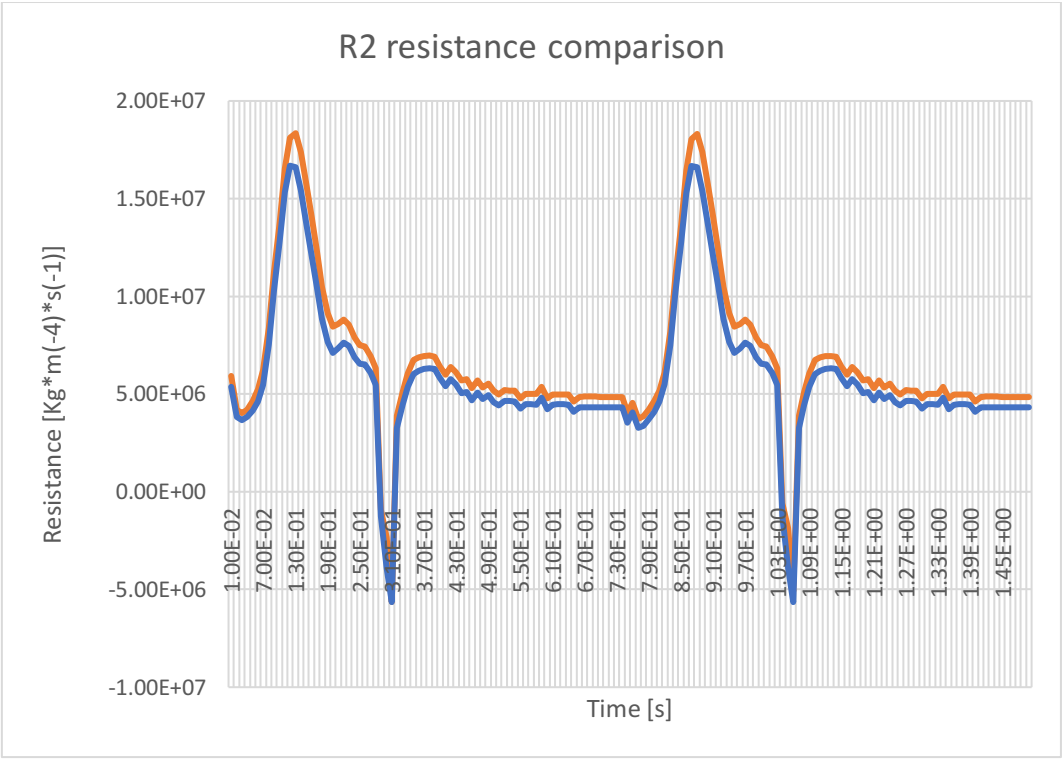

Figure 57. Comparison of resistance values between artery with 1-mm plaques(blue) and healthy artery (orange) in the external carotid artery.

In the common carotid artery (R3), figure 55,and internal artery resistance (R1),figure 56, there appear to be no appreciable variations. The only resistance variation is in correspondence with the internal artery (R2), figure 57, where the case with occlusion again seems to have lower resistance values respect the healty one.

Chapter 4-Discussion

Case under analysis	Maximum WSS [Pa]	location
3-mm Plaque	76.8845	plaque
2-mm Plaque	62.2615	bifurcation
1-mm Plaque	64.9674	bifurcation
Healty case	78.5133	bifurcation

Table2. Maximum values and location of the WSS based on the size of the plates.

Table 2 suggests that the highest WSS value is found in the case of a healthy artery where it is located in the area of the bifurcation mostly adjacent to the external artery. In the case of maximum obstruction however, we do not observe a significant decrease with respect to the healty case, but in this case the maximum values are found in the plaque opposite to the carotid sinus, which therefore seems to be more opposed to the flow. We find an increase in WSS as plate sizes decrease, and a relocation of the WSS at the bifurcation area, index of the fact that the flow in the common carotid artery tends to have a behavior more similar to the healthy case

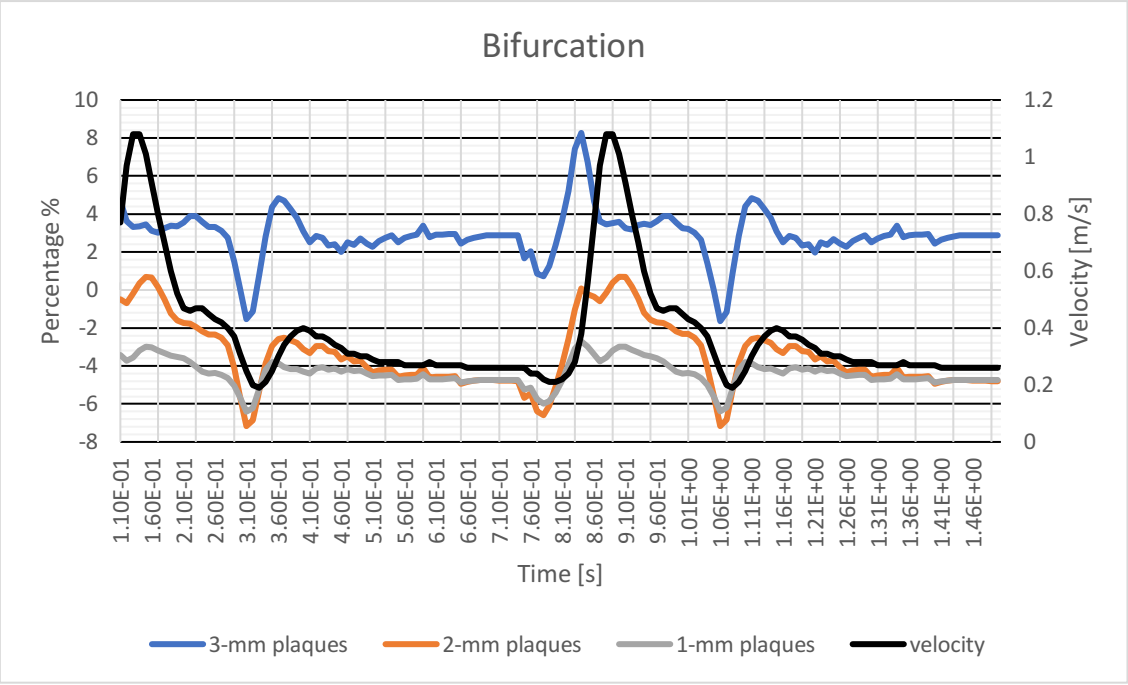

Figure 58. Comparison of the percent change in WSS in the wall_bifurcation as a function of plaque size.

Always referring only to the second cycle, as we can observe from figure 58, the maximum variation in module is approximately 8% found in the case of 3-mm plaques. In fact, a general increase in the WSS is observed in the case of maximum obstruction, while a general decrease is recorded in the other two cases. We note that the maximum percentage variation in the case of maximum obstruction occurs at 0.84s, which

corresponds to a generic time in the phase of speed increase in the systolic phase, time in which the variation of the other two occlusions tends to be minimal. On the other hand, the maximum variation in the case of the other 2 plaques is in correspondence with the minimum speed time (1.07s), where the negative variation is obout 7%. In the phase of constant velocity, therefore in the diastolic phase, the variation in module and the trend is similar in all three cases, presenting a constant variation, in particular, the curves of the two minor obstructions are superimposable. We observe how, however, the variation is greater in the case of 1-mm obstruction than that of 2-mm in the systolic phase. Although the maximum WSS value in the bifurcation with the case of 3-mm plates is lower, the increase in the mean value may indicate that a greater portion of the flow impinges on this area, thereby increasing the mean shear stresses in that area

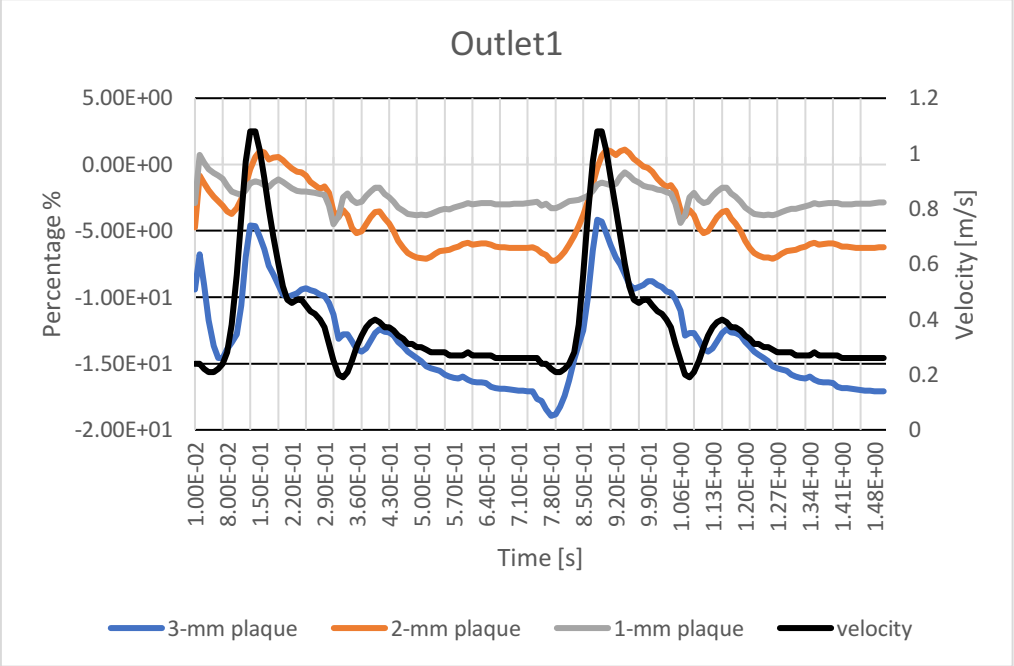

Figure 59. Comparison of the percent change in WSS in wall_outlet1 as a function of plaque size.

Figure 59 highlights how the maximum variation in module is again recorded in the case of maximum occlusion, a negative variation of about 19%, which is therefore much greater than what was recorded in the previous case. The two reduced obstructions, on the other hand, present a variation in modulus more similar to that found in the bifurcation. In this case however, we observe a mostly negative variation for all three cases, although that of the two smaller occlusions is considerably less marked. The two peaks of minimum variation (-5%) which are observed in the case of 3-mm plaques, are found in the times of the maximum velocity of the systolic phase, therefore at 0.13s and 0.8s respectively. The times of greatest variation instead, at 0.79s, corresponds to the end of the diastolic phase. We note how the trend of the 1-mm plaques is not in phase with that reduced of 1-mm, which has a decidedly less constant variation. In this case also the 2-mm plaques shows the maximum mean WSS variation in the same time as the 3-mm plaques, maximum variation of 7%, that of 1-mm instead shows a more or less constant variation of 4%. Negative variations of WSS for the case of maximum occlusion are due both to a lower speed exiting outlet1, and to the fact that the maximum speed no longer tends to be near the wall as in the healthy case, but tends to be more in correspondence of the center of the artery. Although the case of the two minor plates does not present the same variations in velocity compared to the healthy case(in particular the mean velocity of the 1-mm plate

case is not always lower than that of the healty case), it can however be assumed that the velocity near the walls, which therefore influences the WSS, is in any case similar, leading to a comparable variation in WSS.

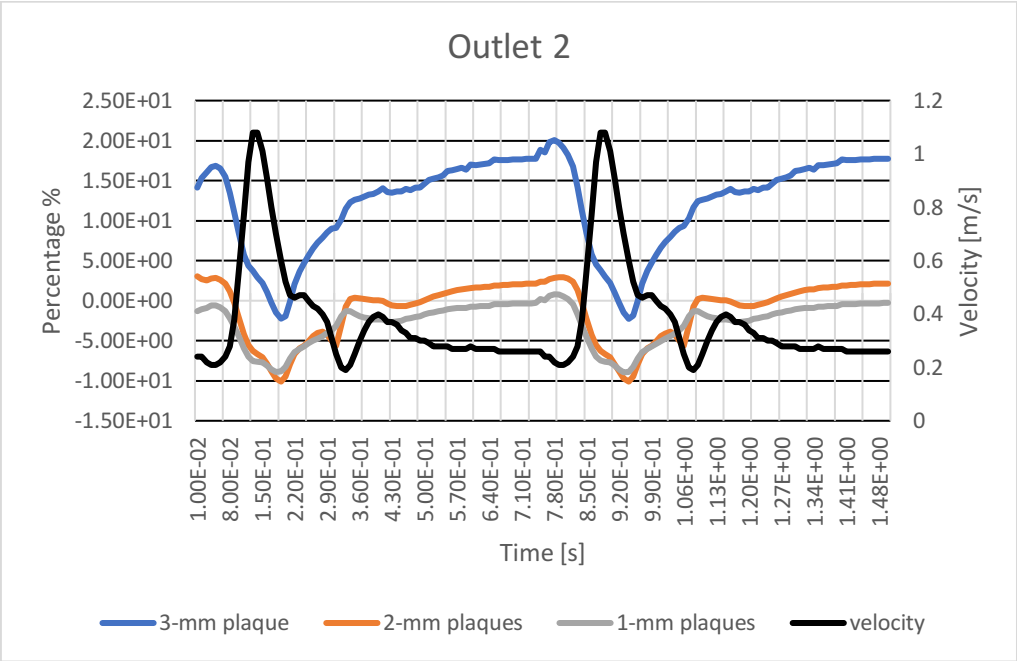

Figure 60. Comparison of the percent change in WSS in wall_outlet2 as a function of plaque size.

Looking at figure 60, at outlet2, therefore in the internal carotid artery, we find instead an increase in the WSS in the case of maximum occlusion, while a general decrease in the other two cases. In particular, it is in this sector that we find the maximum variation of WSS which reaches up to 20% in correspondence with the diastolic phase and therefore before the speed increase phase, instant in which we also found the greatest variation in outlet 1. For the other two occlusions however, a maximum decrease of approximately 10% is observed shortly after the time of the maximum velocity of the systolic phase, time at which, however, the variation in the case of maximum occlusion remains minimal in absolute value. Furthermore, we can observe how in the diastolic phase at constant velocity, the variation in the case of the two reduced occlusions is close to zero, while that of 3 mm plates tends to increase. The increase in this case of 3-mm plaques is easily explained by the fact that the speed exiting outlet2 in the case of 3-mm plaques is much higher compared to the healthy case. For thinner plates the same reasoning as before can be applied, since in this case it is the 2-mm obstruction that generally does not always have lower average velocity values than the healthy case.

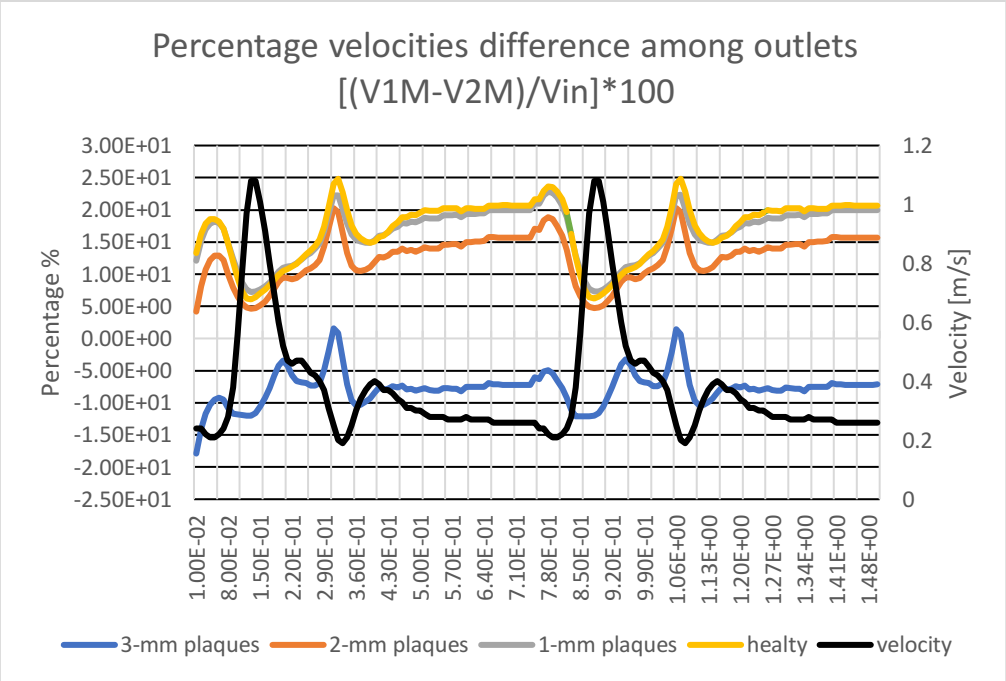

Figure 61. Velocity fraction as function of the size of the plaques.

The top graph of Figure 61 shows the velocity fraction, obtained by subtracting the average exit velocity from outlet 2 from the average exit velocity from outlet 1, then normalized using the incoming speed. We can see that the case of 3-mm plaques is the only one that has an average velocity outgoing from the internal artery (outlet1), which is generally lower than that outgoing from the external artery (outlet2). The greatest fraction (25%) is found in the case of a healthy artery, where the maximum variation is in correspondence with the time of minimum speed, therefore in the diastolic phase, this may be due to the fact that in the diastolic phase, the contribution of velocities in the carotid sinus become more significant. This fraction seems to decrease linearly as the severity of the occlusion decreases, even if in the diastolic phase, the 2-mm plaques

presents a decidedly more marked variation compared to the healty case and 1-mm plaques, a symptom of the fact that the larger plaque has more marked effects on the flow distribution in the diastolic phase. We can, therefore, conclude that a large blockage tends to redistribute the flow on the artery where the blockage is not present, while smaller ones tend to change the speed, but the flow distribution tends to be similar to that of the healthy artery, especially in the case of really small plaques.

Further consideration on the speeds can be made by comparing those obtained from the simulation with those measured in a real case. It has in fact been found, in a healthy bifurcation, that in a state of systole, the external artery (outlet2) generally has higher average speeds than the internal artery (outlet1), a situation which then becomes reversed in the diastolic phase. In our case, this is found only in the diastole phase, a difference most likely due to the fact that the elasticity of the walls has not been included in the model. Furthermore, from the same study, we observe how an occlusion in the carotid sinus tends to decrease the average velocity in the internal artery(outlet1), while it tends to increase it in the external one(outlet2), as found particularly in the case of 3-mm plaques(figure 43)[20].

	Pressure[Pa]		
Case	R1	R2	R3
3-mm plaque	**5,23E+07**	**7,22E+06**	**7,53E+06**
2-mm Plaque	**4,47E+07**	**6,54E+06**	**1,10E+07**
1-mm Plaque	**4,44E+07**	**5,84E+06**	**1,09E+07**
Healty case	**4,44E+07**	**6,63E+06**	**1,17E+07**

Table 3. Mean resistance comparison in the internal artery(R1), external artery(R2) and common artery(R common).

The average resistance values over the two cycles were then calculated. From table3 we observe a general increase in resistance in the internal artery (R1) in the case of 3-mm plaques and 2-mm plaques. On the other hand, a decrease in the common artery resistance (R3) is observed, which is more marked in the case 3-mm plaques. The resistance of the external artery (R2), on the other hand, seems to increase in the case of maximum obstruction and tends to decrease as the size of the plaques decreases, although the values of the 2-mm plaques present values more similar to the healthy case.

As noted in the resistance graphs (figure 35-36-37), in some instants the values took on negative values. This is due to an inversion of the pressure gradient in some instants of minimum speed, albeit small, as shown in the following figure (figure 62). The same figure also shows that this is not due to an inversion of the speed in the outlets.

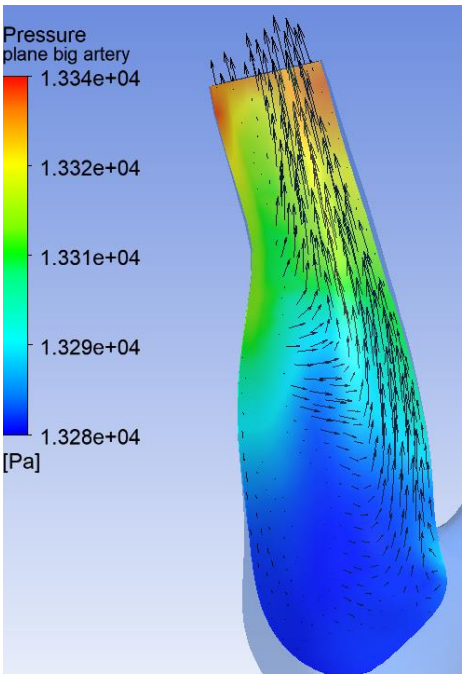

Figure 62. Pressure gradient and velocity vector plot at instant 0.31s.

Conclusions

The healthy bifurcation presents higher maximum WSS values than the respective cases with plates. These values correspond to the area of the bifurcation in all three instants of time analysed. The larger plates, on the other hand, therefore those of 3-mm, are the only ones in which we find maximum WSS values no longer in the bifurcation area, but rather close to the plate. Furthermore, these occlusions are the only ones that generate an increase in the mean WSS in the bifurcation area, a maximum increase of about 8% compared to the healthy case, while the two minor occlusions, therefore of 2-mm and 1-mm, cause a general decrease of approximately 6%. The same trend of the WSS mean variation seems to be present in outlet1, where all three cases of occlusion generate a decrease, even if in the case of 3-mm plates, this decrease reaches values of approximately 19%, while in cases of 2-mm and 1-mm plaques we have maximum variations of 7% and 3%, respectively. On the other hand, it is in outlet2 that we find the greatest differences, in fact in the case of 3-mm plates we observe an increase in the relative WSS of 20%, while the smaller plates cause a maximum decrease of about 9%. This phenomenon can be explained by the fact that only the 3-mm plaques generate a redistribution of the flow in the artery where there is no occlusion, while the other two occlusions, as shown in figure 61, appear to have a fraction of the velocity much more similar to the healthy case. Moreover, it has been seen that the flow profile does not change only downstream of the plaques, but the plaques themselves, opposing the incoming flow, tend to create significant recirculation speeds within the carotid sinus. The estimate of the resistance parameters, suggests that as the occlusion increases, the resistance R1 increases. The R2 resistance instead, does not seem to have a linear trend, in fact the case with 3-mm plaques shows an increase compared to the healthy case, while that of the two minor obstructions, a decrease, which is more marked in the case of 1-mm thick plaques. This may be due to the fact that the maximum pressure values have been extrapolated instead of the average ones, a solution which would have been more correct. R3, on the other hand, decreases both in the case of 3-mm plates and in the case of 2-mm and 1-mm plates, the latter however having values comparable to each other and more similar to the healthy case. The major

limitation of this study is undoubtedly that of not having considered the elastic walls of the vessel, which have significant effects especially on the flow and pressure values, however we concluded that even the geometry alone and its variations have effects on the fluid flow.

Bibliography

[1] Guyton e Hall, in Medical Physiology, Elsevier Saunders, 1956.

[2] D.Savana, G.Heller et all, in Biologia.Blu, Zanichelli, 2011.

[3] CJ. Wiggers, Modern Aspects of Circulation in Health and Disease, 1915.

[4] Major artery of the body, medmovie, https://medmovie.com/topic/cvml_0429a/arterial-anatomy/

[5] C.G.Caro, T.J Pedley, R.C. Schroter, and W.A. Seed. The Mechanics of the circulation. Oxford University Press, 1978

[6] M. G. Schultz, J. E. Davies, A. Hardikar, S. Pitt, M. Moraldo, N. Dhutia, Alun D. Hughes and James E. Sharman. Aortic Reservoir Pressure Corresponds to Cyclic Changes in Aortic Volume. Humans, 2014.

[7] Blausen.com staff Medical gallery of Blausen Medical 2014. *WikiJournal of Medicine*,2014

[8] C.G.Caro, T.J Pedley, R.C. Schroter, and W.A. Seed. The Mechanics of the circulation. Oxford University Press, 1978

[9] Landgraff, Nancy. Cognitive and Physical Performance in Patients with Asymptomatic Carotid Artery Stenosis and Occlusion, 2004

[10] Y. Limbu YR, G. Gurung,R. Malla,R. Rajbhandari ,S. Regmi.Assessment of carotid artery dimensions by ultrasound in non-smoker healthy adults of both sexes. Nepal Med Coll J. 2006.

[11] Li CH, Gao BL, Wang JW, Liu JF, Li H, Yang ST. Hemodynamic Factors Affecting Carotid Sinus Atherosclerotic Stenosis. World Neurosurg. 2019.

[12] S. Glasser, Atherosclerosis: Risk factors and the vascular endothelium, American Heart Journal, 1996.

[13] L. Goldman, A. Shafer, cap.70, in Glodman's Cecil Medicine, 24ª ed., Philadelphia, Elsevier, 2012.

[14] A.Vit,G.De Candia,G. Piccoli , G. Como ,F. Pelizzo ,M. Bazzaocchi . Color-Doppler sonography vs CT-angiography in discriminating carotid atherosclerotic plaques for surgical treatment. A prospective study. Radiol Med. 2003

[15] C. Gopalan, E. Kirk, Chapter 5 - Atherosclerosis, Biology of Cardiovascular and Metabolic ,2022.

[16] F.Santini, Wall shear rate e rimodellamento carotideo: studio mediante nuova metodica multigate doppler, Università degli studi di Pisa, 2008.

[17] C.R. Ethier and C.A. Simmons. Introductory Biomechanics – From Cells to Organisms. Cambridge University Press, 2007.

[18] M. Samaee, M. Tafazzoli-Shadpour, S. Tiari, M. Mahdavi, A novel experimental approach to investigation of blood hemodynamics due to different stenosis severity, Conference: 19th Annual Conference on Mechanical Engineering, 2011.

[19] D.W. Holdsworth, C.J. Norley, R. Frayne, D.A. Steinman and B.K. Rutt, Characterization of Common Carotid Artery Blood-Flow Waveforms in Normal Human Subjects, Physiol Meas,1999.

[20] Alexey V. Kamenskiy, Yuris A. Dzenis, Jason N. MacTaggart, Anastasia S. Desyatova, Iraklis I. Pipinos,In vivo three-dimensional blood velocity profile shapes in the human common, internal, and external carotid arteries, Journal of Vascular Surgery,2011.